RIVISTA DEL NUOVO CIMENTO Vol. 32, N. 11 2009
DOI 10.1393/ncr/i2009-10049-y

Gravity Probe B(*)

G. M. Keiser(1), M. Adams(1), W. J. Bencze(1), R. W. Brumley(1), S. Buchman(1), B. Clarke(1), J. Conklin(1), D. B. DeBra(1), M. Dolphin(1), D. N. Hipkins(1), T. Holmes(1), C. W. F. Everitt(1), J. H. Goebel(1), D. Gill(1), G. B. Green(1), M. Heifetz(1), J. Kolodziejczak(2), J. Li(1), J. Lipa(1), J. M. Lockhart(3), J. C. Mester(1), B. Muhlfelder(1), Y. Ohshima(1), B. W. Parkinson(1), M. Salomon(1), P. Shestople(1), A. S. Silbergleit(1), K. Stahl(1), M. A. Taber(1), J. P. Turneaure(1), S. Wang(1) and P. Worden(1)

(1) *W. W. Hansen Experimental Physics Laboratory, Stanford University Stanford, CA 94305-4085, USA*
(2) *NASA/Marshall Space Flight Center - Huntville, AL 35812, USA*
(3) *Physics and Astronomy Dept., San Francisco State University San Francisco, CA 94132, USA*

Summary. — This paper describes the flight hardware, on-orbit operations, and preliminary data analysis for the Gravity Probe B satellite.

(*) Reproduced from Proceedings of the International School of Physics "Enrico Fermi" Course CLXVIII "Atom Optics and Space Physics" edited by E. Arimondo, W. Ertmer, W. P. Schleich and E. M. Rasel (IOS Press, Amsterdam and SIF, Bologna) 2009, pp. 163-202.

1. – Introduction

On April 20, 2004, at 9:57:24 am PDST, a Delta II 7920-10 rocket lifted off from Vandenberg Air Force Base carrying the Gravity Probe B satellite. Six of the nine solid rocket motors were ignited at liftoff to supplement the main engine, while the remaining three solid rocket motors ignited 62 seconds after liftoff. The rocket arched to the south over the Pacific Ocean with the second stage firing 4 minutes after launch and then cutting off as it passed over the South Pacific. After passing over the South Pole, the second stage was fired a second time to inject the satellite into a 640 km altitude circular polar orbit. Four nitinol-based release mechanisms were heated to deploy the solar arrays. A video camera attached to the second stage confirmed the full deployment of the solar arrays, and the subsequent separation of the satellite from the second stage. These images were relayed to the ground shortly afterwards. With the successful launch and deployment of the solar arrays, the satellite was ready to begin operations.

Using precision gyroscopes in Earth orbit to test Einstein's general theory of relativity was independently proposed by Pugh [1] and Schiff [2, 3] in 1960. Both of these authors pointed out that according to the general theory of relativity, the angular momentum axis of a gyroscope in orbit about the Earth will precess about a direction normal to the orbital plane due to the gravitational interaction of the spinning gyroscope with its orbital motion, and simultaneously about the direction of the Earth's rotation axis due to the interaction of the spinning gyroscope with the angular momentum of the Earth, as shown in fig. 1. The first effect is known as the geodetic effect, and the second is known as the frame-dragging effect. The instantaneous precession rate in Einstein's general relativity for a spherical massive body is given by

$$\boldsymbol{\Omega} = \frac{3GM}{2c^2\boldsymbol{R}^3}(\boldsymbol{R}\times\boldsymbol{v}) + \frac{GI}{c^2\boldsymbol{R}^3}\left[\frac{3\boldsymbol{R}}{\boldsymbol{R}^2}(\omega_e\cdot\boldsymbol{R}) - \boldsymbol{\omega}_e\right]. \tag{1.1}$$

Here G is the gravitational constant, and M, I, and $\boldsymbol{\omega}_e$ are, respectively, the mass, moment of inertia, and the angular rotation rate of a massive body. The vectors $\boldsymbol{R}$ and $\boldsymbol{v}$ are the position and velocity of the gyroscope relative the center of mass of the body. The magnitude of the precession rate due to each of these effects in the vicinity of the Earth is very small. In a 640 km polar orbit, the gyroscope precession due to the orbital motion about the Earth is 6.6 arcsec/y (32 μrad/y), while the orbital average

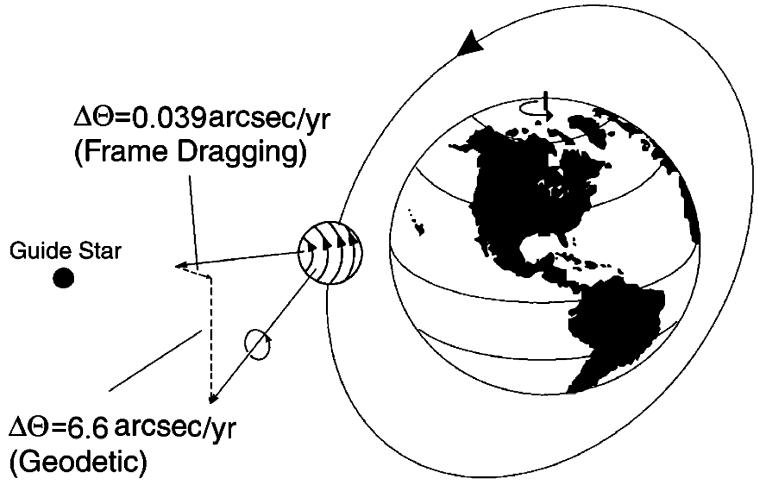

Fig. 1. – Geodetic and frame dragging effects predicted by general relativity.

precession rate due to the Earth's angular momentum is 0.041 arcsec/y (0.20 μrad/y). In addition to the geodetic effect due to the orbital motion about the Earth, there is also a contribution due to the orbital motion about the Sun, where the predicted magnitude is 0.019 arcsec/y (92 nrad/y), and the direction of the precession is perpendicular to the plane of the ecliptic. The magnitude of the solar frame-dragging effect is below the anticipated accuracy of the experiment [4].

The rate of change of the angular momentum, $\boldsymbol{L}$, of a gyroscope is then

$$\frac{\mathrm{d}\boldsymbol{L}}{\mathrm{d}t} = \boldsymbol{\Omega} \times \boldsymbol{L}. \tag{1.2}$$

For the Gravity Probe B gyroscopes, the fractional differences in the moments of inertia $\Delta I/I$ were approximately 3×10^{-6}, so the instantaneous spin axis of each gyroscope lay within 0.6 arcsec (3 μrad) of the angular-momentum axis. Averaged over the herpolhode motion, the spin axis coincides with the angular-momentum axis, and the angular rate of change of a unit vector parallel to this average spin axis is given by

$$\frac{\mathrm{d}s}{\mathrm{d}t} = \boldsymbol{\Omega} \times \boldsymbol{s}. \tag{1.3}$$

In this paper, the left-hand side of this equation is defined as the drift rate whether it is due to relativistic effects or classical torques. Note that the magnitude of the drift rate is only equal to the magnitude of the precession rate, $\boldsymbol{\Omega}$, if the spin axis is perpendicular to the direction of the vector, $\boldsymbol{\Omega}$. As explained below, the spin axis of each of the gyroscopes lay within 30 arcsec (145 μrad) of the direction to the guide star, and it coincided with the orbital plane to within 2.5 arc-min (0.7 mrad). In this configuration, the drift rate of the gyroscope spin axis due to the terrestrial geodetic effect lies in the plane of the satellite orbit (referred to as the North-South direction), and its magnitude is nearly equal to the magnitude of the precession rate. The orbit-averaged drift rate due to the terrestrial frame-dragging effect is perpendicular to the plane of the orbit, and its

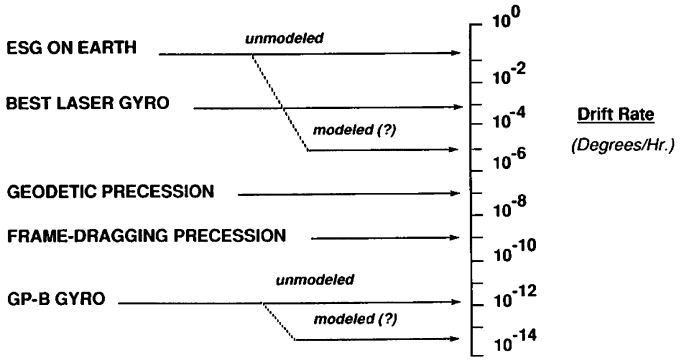

Fig. 2. – Comparison of conventional gyroscopes with Gravity Probe B gyroscope.

predicted magnitude is 0.039 arcsec/y (0.189 μrad/y). Note that for the frame-dragging precession the magnitude of the drift rate is smaller than the magnitude of the precession rate because the gyroscope spin axes are closely aligned with the direction to guide star, which has a declination of 16.84 deg.

The geodetic and frame-dragging effects are respectively analogous to the advance of the perigee and ascending node of the Earth-Moon system in the gravitational field of the Sun first calculated by de Sitter [5], and the motion of the perigee and ascending node of a satellite in the presence of rotating massive body first calculated by Lense and Thirring [6, 7]. Both of these effects are zero in Newtonian gravitational theory. The geodetic effect may be thought of as a direct measure of the curvature of spacetime [8], while the second effect provides direct evidence of a dragging of a local inertial reference frame relative to the distant stars by a rotating massive body.

The performance of a gyroscope may be characterized by its bias stability, read-out noise, and scale factor accuracy [9]. The bias stability sets a floor on the drift rate which can be measured with a gyroscope. Figure 2 compares the bias stability of conventional gyroscopes with the required bias stability of the Gravity Probe B gyroscopes. For ring laser and fiber-optic gyroscopes, the bias stability lies in the range from 1.5×10^{-4} to 15 deg/h [9]. Estimates of the uncompensated bias stability of mechanical Electrostatically Supported Gyroscopes (ESG) are approximately 0.1 deg/h, but this bias stability may be improved by perhaps four orders of magnitude using empirical models to compensate for the bias. By comparison, the drift rate due to the geodetic effect is 10^{-7} deg/h and the drift rate due to the motional effect is 10^{-9} deg/h. The design goal for the Gravity Probe B gyroscopes was an uncompensated bias stability of 3×10^{-12} deg/h (0.1 marcsec/y) and possibly a compensated bias stability of an order of magnitude better.

The most promising means for significantly improving the bias stability of mechanical gyroscopes was to operate the gyroscope in space [1, 3, 10]. For a satellite in a 640 km altitude orbit, the residual acceleration within the satellite is typically 10^{-7} m/s^2 due to the residual air drag and the solar radiation pressure [11]. The residual acceleration may be further reduced by operating the satellite in a drag-free mode where the translation control system of the satellite is operated to keep a proof mass centered within its cavity [1,12]. With an acceleration of 5×10^{-11} m/s^2 in a direction perpendicular to the spin axis of a gyroscope spinning at 80 Hz, the drift rate due to the a mass unbalance torque

is 0.1 marcsec/y (0.5 nrad/y) for a gyroscope with a mass unbalance of 25 nm (The mass unbalance is the displacement between the center of mass and the geometrical center of the nearly spherical gyro rotor projected onto the spin direction of the gyroscope.). At this level, the drift rate is significantly smaller than the estimated statistical error due to readout noise in the experiment.

This example not only illustrates the potential large improvement in the performance of a gyroscope in space but also demonstrates some of the challenges involved. The Gravity Probe B gyroscopes, payload, and satellite were designed so that not only the mass unbalance torque but also all the other classical torques on the gyroscope would be reduced to the level where the disturbance drift rate of the gyroscope spin axis would be less than 0.1 marcsec/y (0.5 nrad/y). Significant reduction in the support dependent torques is possible by operating the gyroscope in a drag-free satellite and by simultaneously reducing other support-independent torques to a corresponding level. It may seem that the requirement for reducing the torques below the level of the statistical readout noise places undue constraints on the design of the satellite since it should be possible to separate the effects of some of the classical torques from the relativistic drift rate. However, the design of the satellite was conservative so as to add a margin of safety to the desired accuracy.

The readout noise and scale factor stability can also contribute to significant performance differences between gyroscopes which directly measure rotation rates, such as laser gyroscopes, and gyroscopes which measure orientation, such as mechanical gyroscopes. For the laser gyroscopes, the readout noise decreases as $1/T^{1/2}$, where T is the measurement time, while the readout noise in mechanical gyroscopes decreases as $1/T^{3/2}$. A typical value for the noise in laser gyroscopes is $10\,\mu\text{deg/h}^{1/2}$ [9], so that a drift rate of $1\,\mu$deg/h could be measured in 100 hours. For the Gravity Probe B gyroscopes, the required readout noise is $0.9\,\mu\text{deg/h}^{3/2}$, so for periods of an hour or less the readout noise is comparable to that of a laser gyroscope. Over longer periods of time, the readout noise of the Gravity Probe B gyroscopes will be significantly smaller. To prevent the scale factor accuracy from limiting the performance of mechanical, integrating gyroscopes, their orientation must be maintained close to null, either by using a gimbaled housing to maintain the readout at null, or, in the case of Gravity Probe B, having a drift rate small enough so that the orientation is effectively maintained close to null.

The initial studies of the feasibility of a satellite to measure these effects started in 1962 [13], and the work on developing the cryogenic gyroscopes and other flight hardware, analyzing potential error sources, and planning the mission began shortly thereafter. This work continued at Stanford University and NASA's Marshall Space Flight Center with progressive improvements in the ground-based performance of the gyroscopes. The Phase B studies for NASA were begun in 1993. In 1995, NASA approved the flight mission, and the work on the flight hardware began.

As understanding of potential sources of error in the experiment improved, it became apparent that one significant source of error was the uncertainty in the proper motion of the guide star. Initial studies had selected Rigel as the guide star, but the uncertainty in its proper motion was ~ 1 marcsec/y with little prospects for improvement. A group at the Harvard-Smithsonian Center for Astrophysics suggested that the guide star should be one that is a radio source as well as an optical source bright enough for the sensitivity needed for the star-tracking telescope on the Gravity Probe B satellite. If the guide star is also a radio source, then its proper motion can be measured relative to extragalactic radio sources using ground-based Very Long Baseline Interferometry (VLBI). More than 1000 potential radio sources were investigated, with the final selection being

IM Pegasi (HR 8703). Initial VLBI observations of the position of the guide star IM Pegasi were made in 1997 [14] and observations continued three or four times per year through 2007 [15]. Combined with earlier measurements by Lestrade *et al.* [16], these observations provided a history of more than 15 years of the location of IM Pegasi relative to the extragalactic reference sources.

From the launch on April 20, 2004, through the end of the experiment initialization phase in August, 2004, flight operations on the Gravity Probe B satellite included initial calibrations of the gyroscopes, set-up of the attitude and translation control systems, a slow spin of the gyroscopes, and finally spin-up of the gyroscopes to their full spin speed. Once the gyroscopes were spinning at their full spin speeds ranging from 61.8 to 82.1 Hz and the final alignment of the gyroscope spin axis to within less than 30 arcsec of the direction to the guide star had been completed, the science data collection phase began. The operations during this period were designed to provide minimal disturbance to the gyroscopes so as to provide a good measure of the relativistic drift rate. From July 17, 2005, through the depletion of the liquid helium of September 29, 2005, a final calibration phase of the experiment took place with spacecraft operations designed to place limits on potential systematic errors.

Analysis of the data collected from launch on April 20, 2004, through the depletion of the liquid helium on September 29, 2005, has been underway for the past two years. Preliminary results were presented at the April, 2007, American Physical Society Meeting in Jacksonville, Florida, [17]. Final results of the data analysis are expected in 2010.

2. – Gravity Probe B flight hardware

The Gravity Probe B gyroscopes were designed to operate at cryogenic liquid-helium temperatures of about 2 K. The benefits of operating at low temperatures included increased mechanical stability, significantly lower gas pressure and hence gyroscope damping torques, and the London moment gyroscope readout described below [18]. Four gyroscopes were mounted in a fused-quartz block metrology reference frame and this quartz block was rigidly mounted to the telescope, which was also operated at cryogenic temperatures and benefited from the improved mechanical stability at low temperatures. The quartz block, with the gyroscopes mounted in cylindrical bores in it and with the fused-quartz telescope bonded to it, was mounted in a low-temperature probe, which served as a vacuum container. The entire probe assembly was inserted into a 2300 L superfluid liquid-helium dewar. The liquid-helium dewar was mounted into the frame of the spacecraft with the attached solar panels, electronics boxes, and communications equipment. Each of these components is described in more detail below. Additional information on the flight hardware may be found in references [19] and [20].

2˙1. *Gyroscope.* – A line drawing of one of the four Gravity Probe B gyroscopes is shown in fig. 3. The fused-quartz rotors were made from Homosil material manufactured by Heraeus-Amersil. Initially the material was ground and polished into cubes, and then the homogeneity of these cubes were initially verified by measuring the uniformity of its index of refraction using a laser interferometer and an index matching fluid [21] and later verified using interferograms supplied by the manufacturer. The cubes of fused quartz were cut into 3.94 cm (1.55 in) diameter spheres using diamond turning followed by grinding with a silicon carbide abrasive. The diameter of each of these rough cut spheres was brought to 3.8011 cm (1.4965 in) and a sphericity of 130–250 nm (5–10 μin) peak-to-valley using a tetrahedral lapping machine with brass lapping heads and an

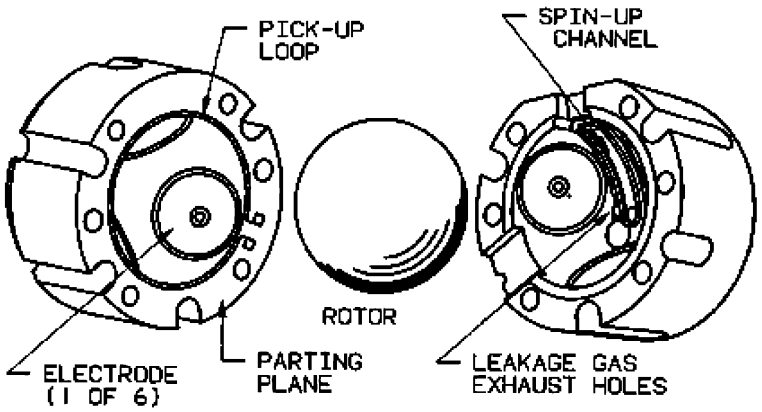

Fig. 3. – The Gravity Probe B gyroscope.

alumina slurry as the lapping compound. It would typically take 20 hours in the lapping machine to bring the spheres to the desired size. Thereafter, the spheres were transferred to a tetrahedral polishing machine, which used phenolic laps and a slurry of cerium oxide polishing compound and water to polish the spheres to within 250 nm (10 μin) of the final size 3.7996 cm (1.4959 in) with a sphericity of better than 25 nm (1 μin). The sphericity of each of the uncoated rotors was deduced from roundness measurements on 17 great circles using a Talyrond roundness measuring instrument manufactured by Rank-Taylor-Hobson [22].

Each of the spheres was coated with a 1.3 μm (50 μin) thick layer of niobium that was uniform to better than 0.3% [23]. This thin layer of niobium provided an electrically conducting surface for the electrostatic suspension system (described below) as well as the superconducting coating for the London moment readout (described below). The required thickness of the layer was driven by the need for a robust coating that could survive a discharge of the electrostatic suspension system during ground-based testing, while the required uniformity of the coating was driven by requirements on the mass unbalance, sphericity, and differences in the moments of inertia of each of the rotors. The uniformity of the coating was achieved by sputter depositing niobium on about 2/3 of the surface of the sphere when the sphere is oriented at each of the faces and vertices of an icosahedron. The thickness of the coating was measured at 26 locations using beta-ray backscattering, and the mass unbalance and differences in the moments of inertia were determined from these thickness measurements. The mass of each of the coated 3.82 cm diameter spheres is 63 g. All the coated fight quality rotors had an asphericity of less than 25 nm (1 μin), a mass unbalance less than 25 nm (1 μin), and fractional difference in the moments of inertia better than 3×10^{-6}.

The gyroscope housing was made from a fused-quartz cylinder with an interior spherical cavity with a radius 31 μm larger than the radius of the coated rotor. The resulting small gap between the rotor and its housing was essential for levitation and testing of the gyroscopes in a 1-g environment prior to integration of the gyroscopes into the flight hardware. The sphericity of each of the uncoated housing cavities as measured by the Talyrond roundness measuring instrument was better than 250 nm.

Other features on the interior of each of the gyroscope housings, as shown in fig. 3, are three pairs of mutually orthogonal electrodes, a gas spin-up channel, and a connector for

charge control of the rotor with ultraviolet light. Each of the electrodes was delineated by a circular cut in the interior of the housing. Within this area, a 2.5 μm (100 μin) thick 7-layer Ti-Cu-...-Cu-Ti electrode was sputter deposited on the surface. The multilayer electrode provides an optically smooth surface and an external layer of Ti which both reduce field emission from the electrode when high (1 kV) voltages were applied to the housing for ground test [24, 25]. Each of the gyroscopes was spun up with a helium gas spin-up system, where the gas flowed through a spin-up channel cut into the housing [26]. The gas entered at the center of the housing, flowed through the spin-up channel, and was pumped out an exhaust line separate from the main vacuum of the probe. In this process, about 97% of the spin-up gas was exhausted through the exhaust line and the remaining 3% of the gas that leaked out of the spin-up channel was exhausted through holes in the housing to the main vacuum probe. It was important to minimize the gas pressure within the housing during spin-up in order to increase the asymptotic spin speed of the gyroscope. A fiber optic cable provided ultraviolet light to the gyroscope rotor. This UV cable terminated at the interior surface of the housing so that the UV light fell both on the interior of the housing and the surface of the rotor. A 2 mm diameter electrode concentric with the termination of the UV cable could be biased at +3, 0, or −3 V to control the direction of the flow of the photoelectrons, thus allowing the rotor charge to be reduced toward zero for both a positive and negative charge on the rotor. To ensure that trapped electrical charges did not provide strong forces and torques on the gyroscopes, a titanium ground plane was sputter deposited on the interior of the housing and electrically grounded through a 300 MΩ resistor to the reference ground for the electrostatic suspension system.

2˙1.1. Gyroscope readout. The gyroscope readout is based on the London magnetic moment of a spinning superconductor [27, 28]. A spinning spherical superconductor spontaneously develops a magnetic dipole moment aligned with its instantaneous spin axis with a magnitude proportional to its spin speed. For a gyroscope spinning at 80 Hz the magnitude of an equivalent uniform field in the center of the sphere is 5.7 nT (57 μG). The changes in the orientation of the gyroscope spin axis may then be determined by measuring the change in the magnetic flux through the 4-turn niobium thin-film pickup loop, which was sputter deposited and lithographically patterned on the parting plane of the gyroscope housing [29]. A superconducting cable connected the pickup loop for each gyroscope to a DC SQUID (Superconducting Quantum Interference Device). With the gyroscope spin axis lying nearly in the plane of the pickup loop, changes in the magnetic flux through the pickup loop are proportional to the angle between the spin axis of the gyroscope and the plane of the pickup loop. To measure the orientation of the gyroscope spin axis to an accuracy of 1 marcsec (5 nrad), it is necessary to measure changes in the magnetic flux through the pickup loop to an accuracy of 3×10^{-20} Wb (3×10^{-12} G-cm^2). Hence, both low noise in the SQUID readout electronics and excellent shielding of the pickup loop from external magnetic fields are needed to reduce the noise of the gyroscope readout system. The SQUID readout electronics and the magnetic shielding are shown in fig. 4.

The London magnetic moment is aligned with the instantaneous spin axis of the gyroscope, and thus it can be used to measure the orientation of the spin axis. Since the London moment is independent of the orientation of the gyroscope spin axis in the body of the rotor, it is not necessary to know or control the orientation of the gyroscope spin axis in the body. Euler's equations of motion determine the time history of the spin axis in the body, and, in the absence of dissipation, the spin axis will continually follow

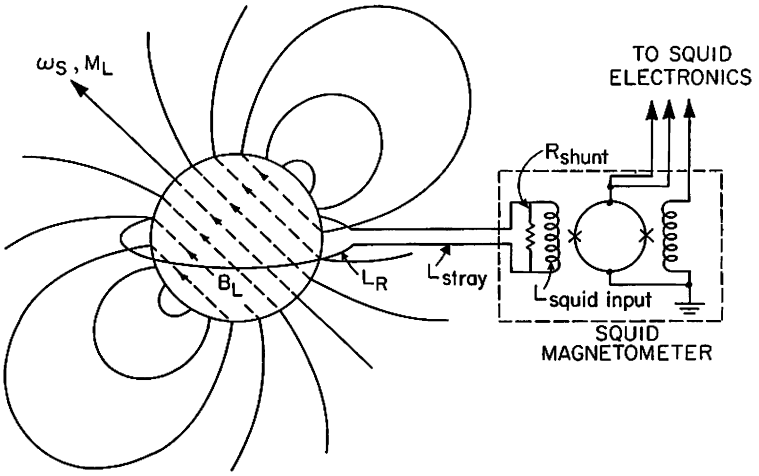

Fig. 4. – Gyroscope readout.

the polhode path determined by the initial conditions and the differences in moments of inertia of the rotor. The fractional differences of the moments of inertia of the Gravity Probe B gyroscope were typically less than 3×10^{-6}, so that at a spin speed of 80 Hz the expected polhode period is greater than 1 h.

As the gyroscope rotors are cooled through their superconducting transition temperature, they trap the residual magnetic field. As opposed to the London moment field, this residual magnetic field is fixed to the rotor's body reference frame. The trapped magnetic field has several important consequences for the Gravity Probe B experiment. First, to maintain the London moment readout as the primary readout for the GP-B experiment, each gyroscope rotor must be cooled in a magnetic field which is small compared to the London moment field. Secondly, as the spin axis follows the polhode path within the rotor, the contribution of the trapped magnetic flux to the gyroscope readout scale factor varies at the polhode frequency. As long as the polhode path remains constant, this periodic modulation of the scale factor will remain constant, but it does complicate the analysis of the data. Finally, the trapped magnetic flux in the spinning rotor produces a rotating magnetic field which provides an excellent method of measuring the gyroscope spin speed. In general, this trapped magnetic field is not a dipole field, so it produces signals at the harmonics of the gyroscope spin speed. Since the spin axis of the gyroscope lies within 30 arcsec (145 μrad) of the plane of the pickup loop, the amplitudes of the odd harmonics of the spin speed are typically 10^4 times larger than the adjacent even harmonics. In addition, the amplitude of each harmonic is modulated at the polhode frequency, so periodic variations in the amplitude of these harmonics can be used to determine the polhode period.

The SQUID readout electronics was designed to measure the magnetic flux applied to the SQUID by the pickup loop circuit. The voltage across a DC SQUID is a periodic function of the magnetic flux applied to the SQUID with a periodicity of the flux quantum, Φ_0. A 420 kHz square wave modulation with a peak-to-peak amplitude of about $\Phi_0/2$ was applied directly to the SQUID. Then, the demodulated voltage across the SQUID is proportional to the difference between the applied magnetic flux and the flux at the appropriate periodic minimum. This demodulated signal is used to produce

a feedback current, which is coupled directly to the pickup loop circuit, to maintain the magnetic flux through that circuit at a constant value. As the magnetic flux from the pickup loop changes due to motion of the gyroscope spin axis relative to the plane of the pickup loop, the feedback current maintains the magnetic flux in the input circuit at a constant value. Then, the change in the feedback current is a direct measure of the change in the applied magnetic flux through the pickup loop.

As the satellite rolls about the direction to the guide star, the magnetic flux through the pickup loop due to the London moment will vary at the satellite roll frequency. The amplitude and phase of this roll frequency signal are a direct measure of the magnitude and direction of the misalignment of the gyroscope spin axis relative to the satellite roll axis, which is approximately aligned toward the apparent position of the guide star. It is this London magnetic moment signal which determines the orientation of the gyroscope spin axis relative to the plane of the pickup loop. In addition to the London magnetic moment signal, there are also signals at harmonics of the gyroscope spin speed due to the trapped magnetic flux. The SQUID readout electronics was designed to preserve the information from both of these sources. A high-frequency channel is digitally sampled at 2200 Hz following a 780 Hz analog low-pass filter, while the low-frequency channel has an additional 4 Hz analog low-pass filter whose output is also digitally sampled at 2200 Hz. A non-causal digital filter further attenuates the high-frequency components of the sampled low-frequency signal before it is included in the telemetry at a 5 samples/s rate.

Since the Gravity Probe B measurement requires such accuracy and dynamic range to measure the rate of change of the orientation of the gyroscope spin axis, one of the concerns in the design of the SQUID readout electronics has been long-term changes in the scale factor of the readout system which, if not measured or carefully controlled, could masquerade as a long-term drift of the gyroscope spin axis. For this reason, a number of provisions were made to measure the stability of the scale factor of the SQUID readout electronics. A calibration signal derived from a voltage reference stable to several parts in 10^5 over one year was injected into the feedback loop and measured by the readout system. In addition, provisions were made to compare the long-term stability of the voltage reference to the flux quantum in the SQUID [30]. The flux-locked loop was opened, and a known voltage offset was used to produce a current, which, when applied to the SQUID, produced an offset of approximately 100 flux quanta. When the flux-locked loop was relocked, the measured feedback current was directly proportional to the difference between the applied signal and the 100 flux quanta signal. By repeating this measurement at regular intervals during the year long data acquisition, long-term changes in the scale factor of the SQUID readout electronics could be measured.

2˙1.2. Electrostatic suspension system. The electrostatic suspension system measured and controlled the position of the rotor relative to each pair of electrodes along a given axis [31]. A capacitance bridge operating at 34 kHz for each electrode axis measured the rotor position relative to the electrodes. A 40 mV peak-to-peak excitation at 34 kHz was applied to each capacitance bridge, while the phase of the excitation on the capacitance bridge for the three electrode axes was shifted by 120 deg to maintain the rotor at a virtual ground. The demodulated potential difference between each electrode pair is a direct measure of the position of the rotor relative to the electrodes. The noise in each capacitance bridge was less than $0.1\,\mathrm{nm}/\sqrt{\mathrm{Hz}}$.

The electrostatic suspension system was required to operate over a wide dynamic range of applied acceleration and force. The pressure from the gas in the spin-up system produced a specific force of approximately 0.1 g with the corresponding voltage applied

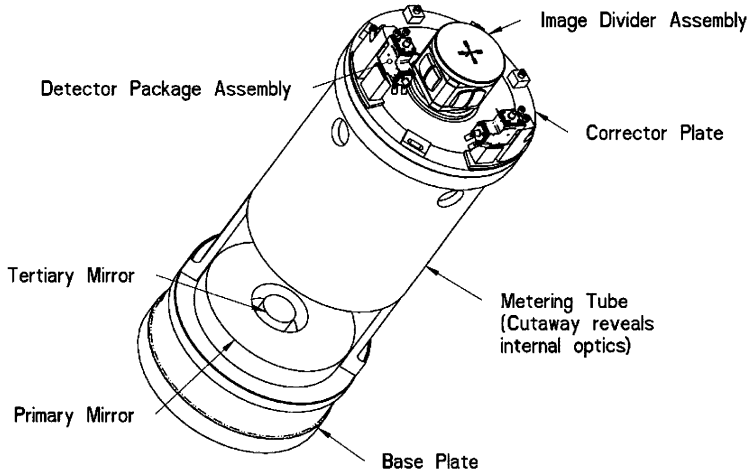

Fig. 5. – Gravity Probe B cryogenic telescope.

to the electrodes of approximately 300 V. After spin up, the quiescent voltages on the electrodes were reduced to 0.2 V to reduce torques due to the electric fields. However, the electrostatic suspension system had to be capable of quickly providing control authority to protect the spinning gyroscopes from a micrometeorite impulse. In addition the suspension system had to be highly reliable since the loss of control on any one of the gyroscopes while it was spinning at high speed would very likely destroy that gyroscope and possibly other parts of the science instrument assembly.

To provide a wide dynamic range, the final amplifier for the electrode voltages was switched between systems with maximum voltages of 750 V (nominally for spin up) and 50 V (nominally during the science data collection). Since the force between two plates of a parallel plate capacitor is proportional to the square of the potential difference, the voltages applied can be either constant or modulated. Calculations showed that the electrostatic torques would be minimized if the voltages were applied equally to each of the three electrode axes, but modulated at 20 Hz with a phase difference between any two axes of 120 deg. To provide flexibility the primary control was implemented digitally, and to provide very high reliability the control would temporarily revert to an analog backup system in case the digital system had a fault.

The electrostatic potential of the rotor was measured by continuously applying a 10 mV sinusoidal bias with a period between 14 and 22 seconds to each electrode pair [32]. The voltages on opposite electrodes were 180^0 out of phase with one another. The resulting force on the rotor at the modulation frequency is then proportional to the rotor potential and can be measured using the control effort signal in the electrostatic suspension system. Each of the three electrode axes provides an independent measurement of the rotor potential.

2˙2. *Telescope*. – The cryogenic telescope [33-35] that was used to measure the orientation of the apparent position of the guide star is a folded Cassegrain telescope with an aperture of 14 cm, a focal length of 3.8 m, and field of view greater than 66 arcsec (320 μrad). The light from the guide star passes through four windows in the cryogenic probe (discussed below). The light from the guide star is reflected from the primary,

secondary, and tertiary mirrors, as shown in fig. 5, and enters an image divider assembly mounted on the front plate of the telescope. Within the image divider assembly, a beam splitter divides the light in half, and each half is focused on the vertex of a roof prism. If the telescope is pointed directly at the star, then light from each roof prism will be divided equally from each side of its vertex. The light beams from each half of a roof prism are sent through another beam splitter and measured by redundant pairs of photodiodes. All of the fused-quartz parts in the telescope and image divider assembly were bonded together using potassium hydroxide bonding. This bonding technique was developed for Gravity Probe B and produced bonds of high strength and reliability [36].

Within the ± 400 marcsec ($10\,\mu$rad) linear range of the telescope, the difference in the measured light from the two sides of the roof prism relative to their sum is a direct measure of the angular deviation of the guide star from the telescope axis. Each pair of photodiodes, which measured the difference in light from both sides of the roof prism, was mounted on a 1.2 cm diameter sapphire platform [37]. Also, mounted on the thermal platform was a two stage JFET preamplifier. This platform was thermally isolated from its base by a polyimide support structure and maintained at 72 K to within 0.1 K. This operating temperature was chosen because it is the temperature of minimum noise performance of the JFETs. The sum of the photocurrents produced by light from the guide star for the four pairs of photodiodes was in the range of 11 to 22 fA with a noise of $0.8\,\mathrm{fA}/\sqrt{\mathrm{Hz}}$. The photocurrent was measured by using a charged-locked loop to maintain the net charge at the input to the preamplifier at null. The compensating charge was provided by applying a feedback voltage across a cryogenic capacitor. The rate of change of the feedback voltage was then proportional to the photoelectric current, and the charged-locked loop was reset every 0.1 seconds. The pointing noise from each of the four channels ranged from 50 to 110 marcsec for each 0.1 s sample. The combined pointing noise from all four detector pairs is then 0.48 marcsec per orbit.

The feedback voltage for the charged locked loop was sampled at a rate of 2200 samples/s and an on-board algorithm determined the rate of change of the feedback voltage. The output of this algorithm was included in the telemetry at a rate of 10 samples/s for each of the eight photodiodes. Each photodiode was sensitive to particle radiation, which would either produce a large offset in the charge-locked loop or saturate the electronics. For this reason it was necessary to eliminate those telemetry data points where there was clearly a charged particle hit. The number of energetic protons in the South Atlantic Anomaly made the telescope readout particularly vulnerable during those times when the satellite passed through this region.

2˙3. *Quartz block metrology frame.* – The telescope was bonded to a fused-quartz block which served as a metrology reference frame as shown in fig. 6. Each of the four gyroscopes was inserted into a cylindrical hole in the quartz block. A fused-quartz index plate and a fused-quartz cylinder accurately located the gyroscope housing so the centers of the gyroscope housings were along a line parallel to the telescope axis to within ± 0.05 mm. The metrology frame aligned the gyroscope assemblies so that the normal to the planes of the pickup loop of gyroscope 1 and gyroscope 2 were parallel to the telescope x-axis, and the normal to the plane of the pickup loop of gyroscope 3 and gyroscope 4 were nearly parallel to the telescope y-axis within 0.6 deg (0.01 rad). The orientation of the spin-up channels for two of the gyroscopes were chosen so that their spin axes were parallel to the direction to the guide star while the spin-up channels of the other two gyroscopes were chosen so that their spin axes were antiparallel to the direction to the guide star.

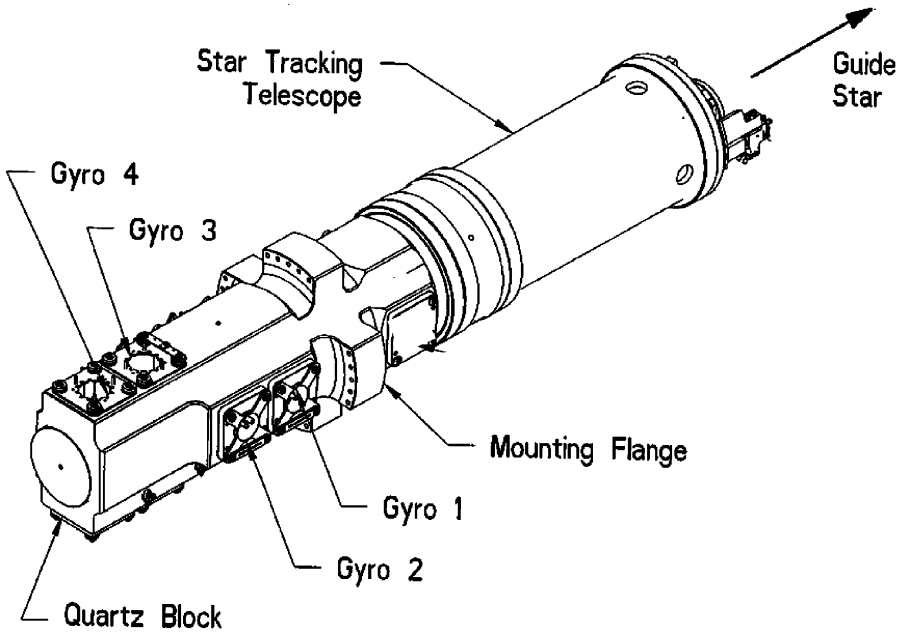

Fig. 6. – The science instrument assembly including the four gyroscopes and the telescope.

2˙4. *Low-temperature probe.* – The fused-quartz block was mounted on the low-temperature vacuum probe, shown in fig. 7, which was designed to be inserted into the superfluid liquid-helium dewar described below. This low-temperature probe also included provisions for the helium spin-up gas and the spin-up exhaust lines. The vacuum feedthrough connectors for the electrostatic suspension system, the SQUID readout system, and instrumentation wires were mounted at the top of the probe and the cables were attached to the interior of the vacuum probe. The overall gas conductance of the vacuum probe was designed to maintain the pressure at the gyroscopes below 0.07 Pa (5×10^{-4} Torr) in the presence of gas which leaked out of the spin-up channels of the gyroscopes. Once the vacuum shell had been installed, the probe could be evacuated and the gyroscopes could be levitated for preliminary room-temperature qualifying tests.

During spin-up of each of the gyroscopes, gate valves were opened at the top of the probe to allow the spin-up gas to be evacuated to space. After the spin-up gas had been turned off, the pressure within the probe reached a level of approximately 10^{-5} Pa (10^{-7} Torr). At this point, the temperature of the interior of the probe was increased from 2 K to 6 K and the desorbed gas was vented to space. To increase the effective surface area of the probe by more than a factor of 5, a sintered titanium cryopump was installed in the interior of the probe in the cryogenic region [38]. After several hours, the gate valves at the top of the probe were closed and the temperature of the interior of the probe and the cryopump were allowed the return to 2 K. Since the remaining helium in the interior of the probe constituted less than one atomic layer on the interior of the probe and the cryopump, and since the effective binding energy of the helium atoms was approximately 150 K [39, 40], as the temperature dropped the remaining helium atoms were absorbed onto the interior surface of the probe and the cryopump. In ground-based tests, the measured residual pressure was shown to be less 10^{-11} Pa (10^{-13} Torr) after

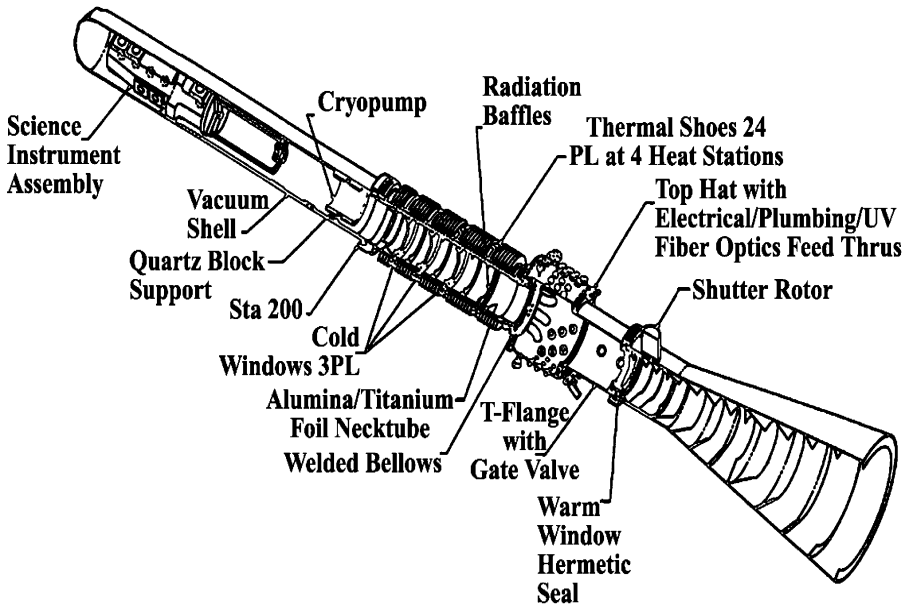

Fig. 7. – The vacuum probe with the science instrument assembly installed.

this low-temperature bakeout. Using this method to reduce the residual gas pressure on orbit effectively reduced the residual gas pressure as a damping mechanism for the gyroscope spin speed to an insignificant level.

2˙5. *Superfluid liquid-helium dewar*. – The low-temperature vacuum probe was inserted into a 2300 L superfluid liquid-helium dewar [41, 42], shown in fig. 8, which was designed to maintain the science instrument assembly at cryogenic temperatures for more than 16.5 months. Boil-off gas from the superfluid liquid helium was exhausted through a porous plug [43] and used to drive 16 proportional thrusters to control the attitude and translation of the spacecraft. To prevent the necessity of transferring superfluid helium on the launchpad, a 4 K normal liquid-helium guard tank intercepted more than 90% of the heat flow into the dewar. The guard tank was emptied after launch.

One of the critical aspects of the liquid-helium dewar was the attenuation of external magnetic fields and the residual magnetic field at the location of the gyroscopes. To prevent interference from external magnetic fields with the London moment readout system, variations in external magnetic fields due to motion of the spacecraft in the Earth's magnetic field had to be reduced by twelve orders of magnitude. Also, to reduce the magnetic flux trapped in the superconducting coating of each of the gyroscopes, the residual magnetic field at the location of each gyroscope needed to be reduced to less than 0.9 nT (9 μG).

These severe requirements on the magnetic field within the probe were met by multiple layers of magnetic shielding. Within the liquid-helium dewar, high-permeability magnetic shielding reduced the residual magnetic field to approximately 0.1 μT (1 mG). A unique lead-tin superconducting shield [44,45] provided further attenuation of external magnetic fields and a stable magnetic field of less than 0.1 nT (1 μG). Rigorous magnetic screening of all materials used in the science instrument assembly and low-temperature probe

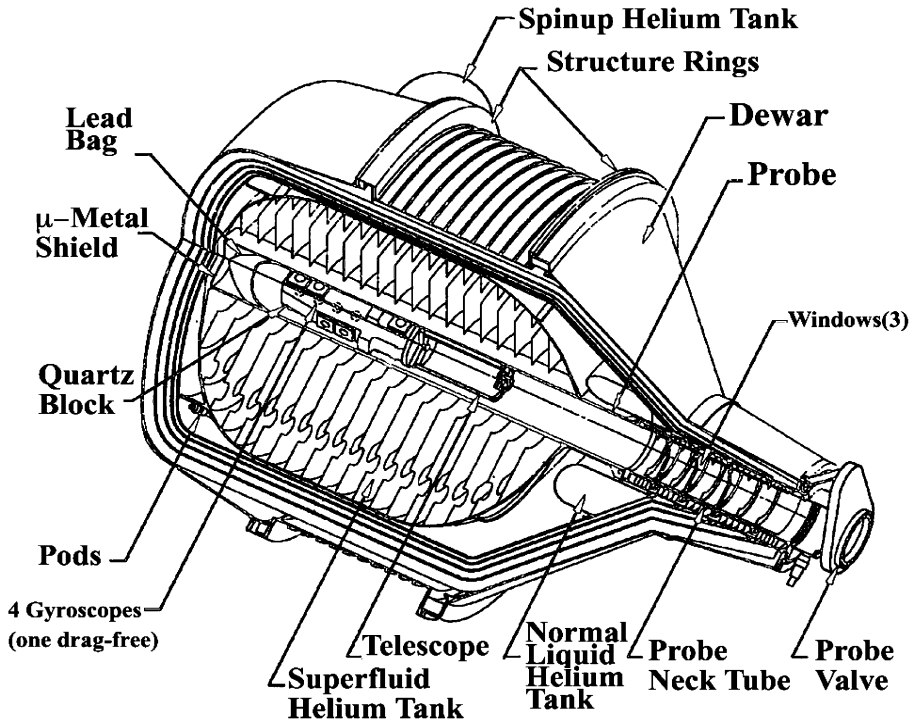

Fig. 8. – The superfluid liquid-helium dewar.

prevented corruption of this residual magnetic field [46, 47]. External magnetic fields were also attenuated by a factor of more than 10^7, limited by distance of each gyroscope from the open end of the cylindrical shield, which had a diameter of 0.2 m and a length of 2 m. Further attenuation of external magnetic fields was achieved by a local cylindrical superconducting niobium shields which were inserted into the bores of quartz block which held each of the gyroscopes, and the shielding provided by the superconducting gyroscope in close proximity to the pickup loop. The measured attenuation of external magnetic fields was greater than 2×10^{-12}.

2˙6. *Spacecraft*. – The superfluid liquid-helium dewar was inserted into an aluminum frame which provided the structural framework for the spacecraft, which is shown in fig. 9. A sunshield was attached to the warm end of the low-temperature probe to prevent the light from the sun from entering the telescope. The specifications for this sunshade were driven by the 22.1 degree ecliptic latitude of the guide star, IM Pegasi. Also, to prevent light from the Earth's albedo from entering the low-temperature probe, a motor driven shutter was mounted above the outermost window of the probe. Power for the spacecraft was provided by four gallium arsenide solar arrays. After launch, the solar array panels were deployed and remained fixed. Batteries provided power to the spacecraft during those times the spacecraft was eclipsed by the Earth. Two omnidirectional antennas, one mounted near the tip of the sunshade and the other mounted on the aft end of the spacecraft provided communication with both the ground stations and NASA's TDRSS satellites. A pair of modified Trimble TANS Vector III GPS receivers [48] were used

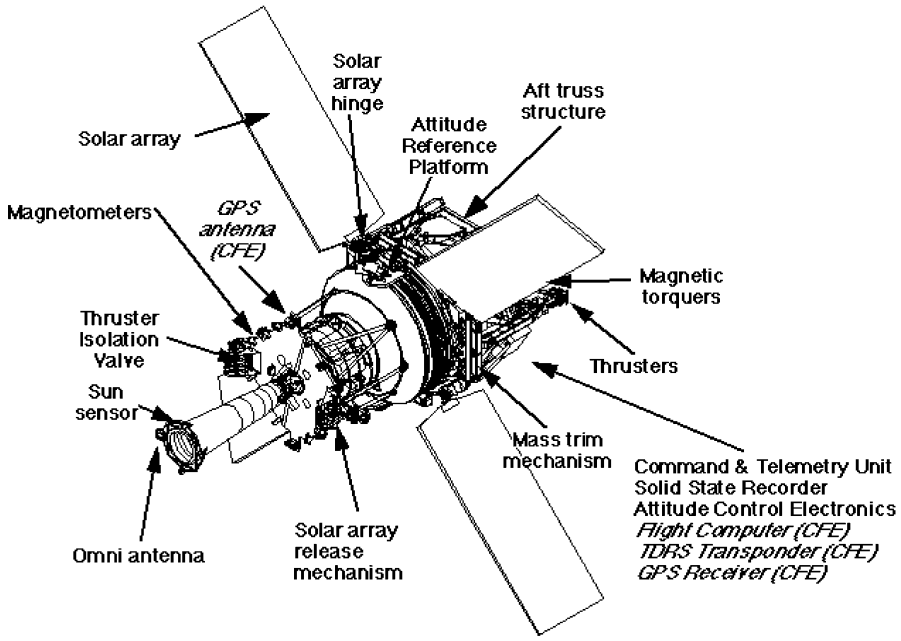

Fig. 9. – The Gravity Probe B spacecraft.

to determine the position and velocity of the spacecraft, and a laser retroreflector was attached to the aft end of the spacecraft.

Particular attention was given to the potential thermal effects on the most sensitive electronics boxes and the mass distribution of the spacecraft. Close to the top of the low-temperature probe where the vacuum feed-through connectors were mounted, which was referred to as the top hat region, a passive thermal shield was designed to enclose the most sensitive electronics boxes. In addition, critical circuit boards within these electronics boxes were temperature controlled. Other electronics boxes, which were less sensitive to temperature and EMI, were mounted near the aft end of the spacecraft. The center of mass for the spacecraft lay between the telescope and the closest gyroscope. Five mass control mechanisms were designed to move 10 or 20 kg masses along thread screws driven by stepper motors to align the principal axes of the spacecraft with the telescope axis and provide a fine adjustment for the radial mass unbalance of the spacecraft. Star tracking telescopes and rate gyroscopes were mounted on attitude reference platforms, which were rigidly attached to the dewar. These sensors were used for roll control and coarse attitude control. When the guide star was visible, the science telescope provided the fine attitude measurement.

3. – Flight operations

3˙1. *Mission operations, communication, and telemetry.* – Although extensive simulations and planning had been conducted in the years prior to launch, the limitations of space-based operations were readily apparent once the satellite was on-orbit. These limitations were principally due to communications and telemetry, but there were also limitations due to scheduling. Although the satellite continued to function 24 hours a

day, it was clear that the scheduling of operations and the communication between teams of people working on the satellite was a key factor. The expertise for each subsystems resided with a few key people, and their availability needed to be included in the planning. After the years of development, there was due caution in all on-orbit operations. With a satellite in orbit, the ground station crew exercised great care in interpreting the data from the satellite and selecting and confirming uploaded commands.

The satellite could send telemetry and receive commands either as it passed over a ground station, or, with limited availability, through NASA's Tracking and Data Relay Satellite System (TDRSS), which relies on 7 geosynchronous satellites to relay telemetry and commands from satellites at lower altitudes. Telemetry sent from the satellite as it passed over a ground station included both data collected during the pass and playback of data recorded on the solid-state recorder. The telemetry rate for data collected during a ground station pass and the rate at which telemetry was recorded to the solid-state recorder was 32 kbits/s. This telemetry was sent over the NASA network to the Mission Operations Center at Stanford University, decommutated, and placed in a database. It usually took two or three hours for this process to be completed. The exception to this rule was telemetry data downloaded during a ground station pass, which was available within minutes. For this reason, most of the critical commands and telemetry were sent and received during a 15 minute ground station pass, or through the TDRSS satellites, so that the effects of the commands could be quickly reviewed. The telemetry data rate through the TDRSS satellites was either 1 kbit/s or 2 kbits/s and depending on the location of the TDRSS satellites relative to the Gravity Probe B satellite, and the available contact time was typically 20 minutes. Scheduling the contacts and planning commands that were to be sent assumed a new importance. Because of the critical time pressure, the Mission Operations Center at Stanford operated 24 hours a day during the initialization phase, with specialized teams working on various aspects of the satellite throughout the day.

A daily operating schedule was established prior to launch which would allow coordination of the many different systems aboard the satellite. A ground station pass was usually scheduled between 4 and 6 am California time (1200 to 1400 GMT) with a playback of the recorded telemetry data over the previous 12 hours. Between the ground station pass and 8 am California time (1600 GMT), the telemetry data was transferred over the I/O net, decommutated, and stored in the telemetry database ready for review. Between 8 and 10 am, the telemetry was reviewed and a short report was prepared by the 8 teams for the All Hands Meeting at 10:00 am. The thirty to forty minute meeting included discussion of the previous day's activities, reports from the various subsystems, and a discussion of operations planned for the following day. An 11:00 am planning meeting filled out the details of the stored program commands which would be sent to the spacecraft that evening. In the afternoon, the detailed sequence of stored program commands was scheduled, followed by a sign-off meeting at 4:00 pm. As long as no problems were discovered at the sign-off meeting, the stored program commands for the next 24 hours were uploaded to the satellite during the next available ground station pass.

The telemetry information from the satellite included both engineering monitors designed to verify the proper operation of various spacecraft components, and science monitors used to determine the orientation and drift rate of each of the gyroscopes relative to the guide star and to place limits on potential systematic errors. The rate at which telemetry information could be recorded to the solid-state recorder, for later transmission to the ground, was 32 kbits/s. Half of this telemetry rate was allocated to high-bandwidth snapshots from the critical subsystems, and the other half was allocated to regular trans-

mission of individual telemetry monitors. The snapshot data from the SQUID readout system or the telescope readout system was collected at 2200 samples/s for an interval of 2 seconds. Snapshot data from the electrostatic suspension system was collected at 220 samples/s for intervals up to 10 seconds. These high rate snapshots provided a digital oscilloscope which could be used for both diagnosis and later detailed analysis.

There were more than 10000 individual telemetry monitors which were routinely sent to the satellite's flight computer. Of these, more than 1000 were included in the telemetry format table and recorded to the solid-state recorder. During each 0.1 s interval, one line of the telemetry format table was stored in the solid-state recorder. Each line consisted of 192 bytes with the first five bytes identifying the vehicle time at which the information was stored in the solid-state recorder. Each telemetry format table consisted of 100 rows so the slowest rate at which any one monitor could be included in the stored telemetry was once every 10 seconds (0.1 samples/s), while the fastest rate was once every 0.1 s (10 samples/s). Because of these rate limitations, it was essential to compress the data using digital filters or the on-board Fast Fourier Transform algorithms, so that the available data could be included in the recorded telemetry. These telemetry format tables could be changed during flight.

3˙2. *Mission phases.* – The mission was divided into three distinct phases. The initialization phase, or Initial On-orbit Commissioning, began immediately after launch and ended after 4 months when the gyroscopes were spun up to their full spin speed and their final alignment had been completed. During the science data collection phase, which lasted for 11.5 months, the disturbances to the gyroscopes were kept to a minimum and information on the orientation of the gyroscopes was continuously collected. Finally, we entered a calibration phase for the final month and a half of the mission. During this phase, the operating conditions of the gyroscopes and the spacecraft were deliberately changed to place limits on the potential systematic experiment errors.

3˙2.1. Initialization phase. The initialization phase consisted of the initial check out of the various subsystems and extensive operations with the spacecraft's attitude and translation control system. It included acquisition of the guide star, adjustment to the attitude control system to allow rapid reacquisition of the guide star following its occultation by the Earth every orbit, and tests of the various operating modes of the drag-free control system. The electrostatic suspension system was used to levitate the gyroscopes and measure the rotor potential. Then, the ultraviolet charge control system was used to discharge the gyroscopes. The initialization phase offered a unique opportunity to measure the thermal sensitivity of the gyroscope readout system while each rotor was electrostatically caged. The residual trapped magnetic flux in each of the rotors was measured, and a planned magnetic flux reduction procedure, which consisted of heating the gyroscopes above the superconducting transition temperature and slowly cooling them again, was used to reduce the trapped magnetic flux in the gyroscope rotors. Before spinning each of the gyroscopes, tests of planned calibration procedures that would entail more risk with a spinning gyroscope were carried out. Before spinning each gyroscope up to its full speed, they were spun up to 3 Hz to test the spin-up procedures and the operation of the electrostatic suspension system with a spinning gyroscope. Finally, each gyroscope was spun up to its full speed. Low-temperature bakeout was used to decrease the residual gas pressure within the probe, and the final alignment of the spin axes of each of the four gyroscopes were made. Each of these operations is described in more detail below.

Initial tests of the liquid-helium boil-off rate on orbit showed that the dewar lifetime would be in the range of 16 to 18 months [49]. Nevertheless, there was a constant sense of urgency to begin collecting the data on the drift rate of the gyroscopes spinning at full speed. For this reason, the initialization phase was planned for 60 days, but the specific tasks were scheduled so that they could be completed in 40 days. However, the initialization phase was only completed after 123 days with three out of the four gyroscopes spinning at full speed and aligned on August 28, 2004 and the completion of the final alignment of gyroscope 4 on September 13, 2004. The increased length of the initialization phase was due to the limited communication with the satellite, the caution in all on-orbit operations, and the longer than anticipated time required to adjust the control systems of the payload and satellite.

Guide star acquisition. – The roll control and coarse attitude control for the Gravity Probe B spacecraft relied on the star trackers and rate gyroscopes, which were mounted on the attitude reference platforms, which were designed to be mechanically stable with respect to the fused-quartz block, the metrology frame for the science instrument. Prior to the initial guide star acquisition and during those times where the guide star was occulted by the Earth, these sensors were used to determine the spacecraft's attitude. Once the guide star was within the 1 arc-min (0.3 mrad) field of view of the cryogenic science telescope, it was used, along with one of the rate gyroscopes and the two star trackers, to bring the spacecraft to within the ± 400 marcsec (1.9 μrad) linear range of the science telescope.

One of the difficulties of this attitude control system was that the pitch and yaw determination showed a larger than expected thermal sensitivity, so when the guide star was visible again after being occulted by the Earth, the attitude was farther from the guide star with the result that the acquisition time was longer than desired. This difficulty was solved by adjusting the bias in the pitch and yaw estimators from time to time (on the order of days) so the spacecraft's attitude nearly aligned the telescope axis with the direction to the guide star upon reacquisition of the guide star. With these adjustments, the time required to drive the spacecraft attitude to within the linear range of the telescope was less than 2 minutes. During the 56 minutes of each orbit where the guide star was visible, the telescope optical axis and the satellite roll axis typically remained within 200 marcsec (1 μrad) r.m.s. of the apparent direction to the guide star. During the remaining 42 minutes, when the guide star was eclipsed by the Earth, the rate gyroscope and star trackers typically kept the satellite roll axis within 10 arcsec (50 μrad) of the direction to the guide star.

Orbit determination and trim. – The position and velocity of the Gravity Probe B spacecraft was determined at 10 s intervals by an onboard GPS receiver [50, 51]. Data collected with overlapping 30 h intervals were fit to a geopotential model which included terms up to degree and order 35. This ephemeris information was used for spacecraft operations as well as three critical aspects of the data analysis: the optical aberration of the guide star position due to the orbital motion of the spacecraft about the Earth, the predicted effects of general relativity for the actual Gravity Probe B orbit, and an independent estimate of the acceleration of each of the gyroscopes due to the gradient in the Earth's gravitational field. The overall accuracy of the orbit determination was a position error of better than 3 m and velocity error of better than 4 mm/s. This orbit determination with the on-board GPS receivers was confirmed with ground-based laser ranging measurements using the satellite retroreflectors. With this position and velocity accuracy, the optical aberration due to the spacecraft's orbital motion and the predicted relativistic

effects could be determined to a fractional accuracy of better than 1 part in 10^5.

One of the reasons that the polar orbit for the Gravity Probe B satellite was selected was to minimize the disturbances to the supported gyroscopes due to the gradient in the Earth's gravitational field. The radial gradient in the Earth's gravitational field at an altitude of 640 km is $2.3 \times 10^{-6}\,\mathrm{s}^{-2}$. The separation between each adjacent gyroscope along the satellite roll axis is 82.5 mm. For a gyroscope which is 165 mm from the drag-free gyroscope, the gradient in the Earth's gravitational field will produce a specific force of $3.8 \times 10^{-7}\,\mathrm{m/s}^2$. If all four gyroscopes lie in the orbit plane, then this gravity gradient force on each of the gyroscopes will average to zero. For non-polar orbits, the regression of the orbit plane will slowly change the orbit plane relative to the fixed orientation of the satellite roll axis. However, even for a polar orbit, perturbations on the orbit due to the sun and the moon will gradually change the orbit. For this reason, the initial orbit was selected so that the average gravity gradient perturbation along with the measured mass unbalance and asphericity of each rotor produced a drift rate of less than 0.1 mas/y. Calculations of the perturbations of the orbit indicated a range of co-inclinations and ascending nodes which would meet this requirement. Since the Delta II rocket could not guarantee orbit injection to the required level of accuracy, provisions were made to trim the orbit using the helium thrusters. However, initial determinations of the orbit showed that the orbit was well within specification and the orbit trim was not necessary.

Drag-free control. – The drag-free control system was used to reduce inertially-fixed accelerations transverse to the satellite roll axis to less than $2 \times 10^{-11}\,\mathrm{m/s}^2$ in the frequency band from less than 0.01 mHz to 10 mHz [51,52]. The principal errors are housing related and spectrally shifted by the satellite roll. There were two operating modes of the drag-free control system. In one case, the control voltages for the electrostatic suspension system on one gyroscope were turned off, and only the 34 kHz suspension bridge was turned on to measure the position of the housing with respect to the rotor. This position signal was sent to the spacecraft's translation control system, which was used to drive the output of the capacitance bridge to zero. In the second case, the control voltages of the electrostatic suspension system remained active with a 20 Hz sinusoidal voltage with an amplitude of 0.2 V applied to each of the six electrodes. As long as the electrostatic forces due to the two electrodes on a given axis were equal, there was no net force on the rotor. The control effort signal, which adjusted the net force on the rotor, was sent to the spacecraft's translation control system. The translation control system then drove the net force on the drag-free gyroscope to null. The drag-free errors at the low satellite roll frequency were comparable for both modes. However, because of the higher reliability and safety, this second operating mode was used for the majority of the mission.

Magnetic flux reduction. – During the ground-based acoustic tests on the spacecraft prior to launch, the residual trapped magnetic field in each of the gyroscopes increased. The low trapped magnetic field in each of the gyroscopes could be restored by heating the gyroscopes above their superconducting transition temperature and slowly cooling them again through the transition temperature. Because of these test results, a similar operation was planned on-orbit. Indeed, the first on-orbit measurements of the trapped magnetic flux showed that each of the four gyroscopes had a residual magnetic field in the range from 0.1 to 0.2 nT (10 to 20 μG). Each of the gyroscopes was heated above its superconducting transition temperature and then allowed to slowly cool through the transition temperature again. This cycle was done carefully to avoid heating the main superconducting shield above its transition temperature. This operation had a significant impact on the operation of the thrusters since the amount of boil-off gas from the liquid-

helium dewar increases from less than 10 mg/s to 27 mg/s [49]. This boil-off gas exceeded the design requirements of the proportional thrusters and may have contributed to a failure of one of the 16 thrusters. Fortunately, the remaining thrusters could adequately control the spacecraft. The dipole equivalent trapped magnetic flux in each of the four gyroscopes was reduced to less than 0.3 nT (3 μG) for gyroscope 1, which is closest to the mouth of the large superconducting magnetic shield, and to less than 0.02 nT (0.2 μG) for gyroscope 4. From these results, it was clear that the low magnetic-field region within the superconducting lead foil magnetic field had not changed during launch.

Gyroscope spin-up and low-temperature bakeout. – Spinning up the four gyroscopes was the on-orbit operation with the highest risk. A failure of the electrostatic suspension system during spin-up could cause the gyroscope spinning at high speed to collide with the wall of the housing. Such a collision would almost certainly destroy the gyroscope, and the debris may have interfered with the operation of the other three gyroscopes. For this reason, the spin-up of each of the four gyroscopes were done in steps: the gyroscopes were initially spun at several tenths of a Hz, then at 3–5 Hz and finally spun to the full spin speed. Between each of these steps, there was a period of several weeks where the measurement of the spin speed and spin-down rate as well as the polhode period could be carried out, and confidence in the reliable operation of the electrostatic suspension system was established.

As each of the gyroscopes was spun to its final spin speed, there was a decrease in the spin speed of the other three gyroscopes because of the helium gas pressure within the low-temperature probe. The final spin speeds of the four gyroscopes were 79.4, 61.8, 82.1, and 64.9 Hz. After the residual gas was evacuated to space, the measured spin-down rate of each of the four gyroscopes indicated the pressure was approximately 10^{-6} Pa (10^{-8} Torr). At this point, each of the four gyroscopes, the interior of the vacuum probe, and the sintered titanium cryopump were heated from 2 K to 6 K. The gate valve at the top of the probe was opened to space for a period of 8 hours. Then, the valve was closed, the heaters were turned off, and the interior of the probe was allowed to cool to 2 K. After this low-temperature bakeout operation, the measured spin-down time constants for the four gyroscopes ranged from 0.29 to 1.4 μHz/h, indicating that the pressure was less than 2.0×10^{-9} Pa (1.5×10^{-11} Torr). The remaining helium gas had been adsorbed onto the surface of the cryopump and the interior of the probe. However, differences in the spin-down time constants of the four gyroscopes and the lack of observable variation in the spin-down time constant with temperature indicated that the residual gas pressure was not the dominant spin-down torque acting on the gyroscopes. Later tests confirmed a pressure of approximately 10^{-12} Pa (10^{-14} Torr).

Gyroscope spin axis alignment. – One final operation before beginning the science data collection phase was to nudge the spin axis of each of the four gyroscopes closer to the desired alignment, so the average misalignment between the gyroscope spin axis and the satellite roll axis over the course of the year was expected to be less than 10 arcsec (50 μrad). A torque was applied to each of the four gyroscopes by taking advantage of the equatorial bulge of approximately 25 nm asphericity of the rotors due to the combined effects of the centrifugal forces and the static rotor shape. By increasing the preload voltages on each of the axes of the electrostatic suspension system to 50 V, and by modulating this voltage at the satellite roll frequency on the two electrode axes which lay at 45 deg to the spin axis, the electrostatic torque applied to the rotors produced a drift rate of the gyroscope spin axis of 3 arcsec/h (15 μrad/h). The direction of this gyroscope drift rate could be changed by changing the phase of the modulation of the

average voltage on each electrode axis. As the spin axis of each gyroscope neared its goal, this average voltage was decreased to 8 V, reducing the drift rate to less than 0.08 arcsec/h (0.4 μrad/h). Once each gyroscope had reached the desired orientation, this torque was effectively removed by reducing the voltage to 0.2 V, and maintaining the average voltage constant to better than 1 part in 10^5.

3˙2.2. Science data collection. The science data collection on gyroscopes 1, 2, and 3 began on August 28, 2004, and on September 13, 2004 for gyroscope 4, because of the additional time required to nudge the spin axis into its final orientation. At this point, the operation of the spacecraft became more routine. Telemetry data was transmitted to a ground station approximately two or three times a day, and a set of commands was uploaded every few days. These commands included the selection of the snapshot data to be recorded to the solid-state recorder, a scheduling of the transmission to the ground station, and other routine operations of the spacecraft. However, the intent was to disturb the science gyroscopes as little as possible, so as to collect adequate data to determine the orientation of the gyroscope relative to the guide star.

The telemetry data were reviewed on a daily basis. The daily all-hands meeting included reports on the operation of the spacecraft power system, attitude and translation control, and orbit determination. To determine the orientation of the gyroscope spin axis relative to the guide star, the most important telemetry data were those from the gyroscope and telescope readout systems and the roll phase measurements. This data was reviewed every morning and used to determine the orientation of the gyroscope spin axis as described in the section on data analysis below. Also important was the telemetry from the electrostatic suspension system on the voltage applied to each of the electrodes and the information on the electrostatic potential of the rotor. The telemetry from the GPS receiver was monitored to ensure that the position and velocity information was adequate and the time of the primary vehicle clock could be determined relative to the GPS time. Particular attention was paid to the temperatures of the electronics boxes, some of the electronics boards within the boxes, and the temperature of the SQUID, the photodiodes, and the cryogenic region close to the science instrument assembly. Information from the snapshots and the Fast Fourier Transform (FFT) of data from the high-frequency channel was used to monitor the gyroscope spin speed and the polhode period which were determined from the frequency and amplitude of the signals at harmonics of the spin speed for each gyroscope.

Within weeks of the beginning of the science data collection phase, it became evident that the polhode period of each of the four gyroscopes was changing with time. This polhode period was determined from the modulation of the amplitude of each of the harmonics of the gyroscope spin speed. Figure 10 shows a plot of the polhode frequency as a function of time for each of the four gyroscopes over the year following the spin up of the gyroscopes to their full spin speed. This changing polhode period indicated that the polhode path of the spin axis within each of the gyroscopes was slowly damping toward the direction of the principal axis of the maximum moment of inertia. As can be seen from this figure, the polhode frequency of gyroscopes 1 and 2 showed a cusp, indicating that the spin axis of each of these gyroscopes had passed through the separatrix, so that the polhode path has made a transition from revolving about the axis of the minimum moment of inertia to revolving about the axis of maximum moment of inertia. Although this changing polhode path would have no impact on the London moment signal, it would slowly change the small contribution of the trapped magnetic flux to the total gyroscope readout signal.

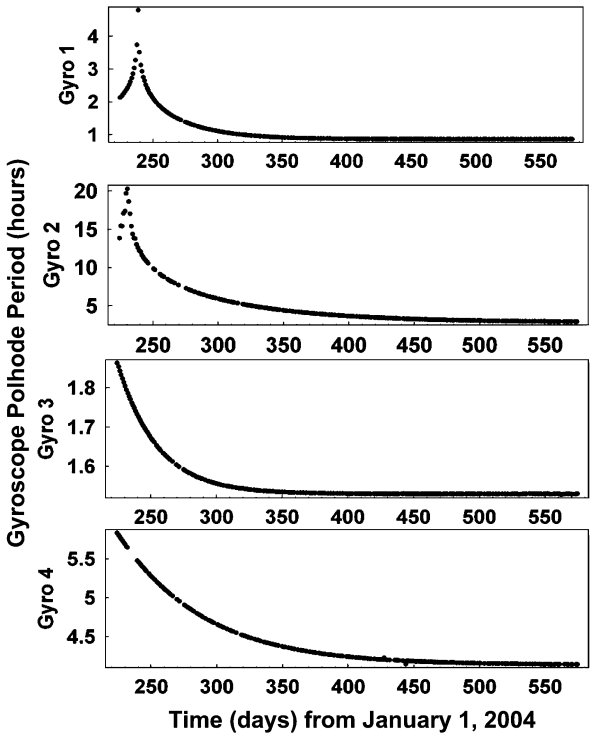

Fig. 10. – Polhode period for of the four gyroscopes.

During the science data collection phase, the standard operations were interrupted a total of 9 times because of spacecraft anomalies. These anomalies to the normal operation of the spacecraft were due to a variety of causes, the most frequent one being a reboot of the spacecraft's flight computer probably due to charged particle radiation. Another example is the anomaly which began on January 20, 2005, where the incidence of the solar proton flux with energies greater that 10 Mev increased from less than 0.1 to greater than 100 particles/(cm^2-s-sr) for several hours, only returning to within a factor of 10 of its quiescent level only after a day and a half. The flux of protons and secondary particles was high enough so that the telescope photodiodes were receiving particle hits at a rate higher than their 10 Hz reset rate. The signal from the science telescope was not usable, and the attitude control system had to rely on the star trackers and rate gyroscope. Over the course of one day the satellite roll axis drifted approximately 2 arc-min (3 mrad) from the guide star before the particle radiation had decreased to a level where the telescope signal was usable. Even then it took sometime to reacquire the guide star and re-establish the normal operating conditions. The loss of data during these anomalies was not as much of a concern as the possibility of larger than expected torques acting on the gyroscopes. The data from each of these anomalies is being carefully evaluated to determine the extent to which additional parameters have to be included in the data analysis to account for any offset in the orientation of the gyroscope spin axis during these periods.

3˙2.3. Calibration phase operations. In any high-precision laboratory experiment it is important to vary the conditions of the experiment to determine if they have any influence on the measured results. Large changes in the operational conditions are most useful since they would clearly indicate whether any one of the changes has a significant effect on the measurement. For an experiment in space, there is the additional concern that significant changes in the operating conditions will inadvertently cause a failure of a critical component. For this reason, after spin-up of the gyroscopes the emphasis was on collecting the data needed to determine the gyroscope drift rate. Only after an adequate amount of data had been collected were the operations designed to place limits on potential systematic errors begun.

These operations were divided into three groups. The first group of calibrations, known as the Phase 0 Calibrations, is a group of low-risk operations that were not expected to have a significant impact on the data or, at worst, would cause a temporary loss of data. These operations included changing the bias of the SQUID readout system, changing the frequency and amplitude of the calibration signal injected into the readout system, turning off or changing the set point of the temperature control on critical circuit boards and the SQUID itself. All of these operations provided valuable information on potential systematic errors, which must be accounted for in the analysis of the data. Limited Phase 0 Calibrations were started on May 15, 2005.

A second group of operations, known as Phase 1 Calibrations, is a group of operations which were expected to significantly increase on the classical torques acting on the gyroscopes. These operations included increasing the average voltages on the electrostatic suspension system, deliberately modulating these increased preload voltages at the satellite roll frequency, changing the position of the gyroscope within the housing, and deliberately modulating the position of the gyroscope at the satellite roll frequency. Since these operations could be performed on individual gyroscopes, they were started on July 18, 2005, on gyroscopes 2 and 3, while gyroscopes 1 and 4 were undisturbed.

The third group of calibrations involved the entire spacecraft. Since these calibrations might influence the drift rate of all four gyroscopes, they were not begun until August 15, 2005. These operations included deliberately accelerating the spacecraft up to the 10^{-7} g capability of the thrusters to determine gyroscope torques proportional to the residual acceleration. In addition, the orientation of the satellite roll axis was deliberately changed to place limits on gyroscope torques which were proportional to the misalignment between the spacecraft roll axis and the gyroscope spin axis. In these operations, the spacecraft's attitude control system was commanded to move the satellite roll axis to a direction of another star, acquire the star and remain in that orientation for up to one day, and then return to the guide star, IM Pegasi. A total of 17 different maneuvers were made with the majority of maneuvers to stars or virtual stars within 1 degree of the guide star. At the same time, the operating conditions were changed: the control voltages of the electrostatic suspension system were changed to d.c. from the a.c. modulated at 20 Hz and the spacecraft was deliberately accelerated in an inertial direction perpendicular to its roll axis. In the final days of the calibration phase, the satellite roll rate was decreased to search for additional potential systematic errors that depended on the satellite roll rate. On September 29, 2005, the increasing temperature of the science instrument assembly and the increasing spin down rate of the gyroscopes due to the increasing pressure signaled the depletion of the liquid helium.

4. – Analysis of flight data

More than a terabyte of telemetry data was collected from the Gravity Probe B satellite during its year and a half of operation. The majority of this data was from the science instrument assembly which was used to determine a continuous time history of the orientation of the gyroscopes relative to the guide star, IM Pegasi and to place limits on potential systematic errors. During the science data acquisition phase of the mission operations, preliminary estimates of the orientations of each of the gyroscope spin axes were made, and this information was used in the planning for the calibration phase operations. After the depletion of the liquid helium on the spacecraft, a more detailed analysis of data was begun. The results presented here are preliminary results. More complete and accurate results are expected by 2010.

4˙1. *Determination of gyroscope spin axis orientation relative to guide star.* – Measurements of both the orientation of the gyroscope spin axis and the apparent direction to the guide star are made relative to the quartz block metrology reference frame. The SQUID readout electronics provides the signal which determines the orientation of each of the gyroscope spin axes with respect to the quartz block, and the telescope readout electronics provides the signals used to determine the apparent orientation of the guide star with respect to the quartz block. Since the entire spacecraft, including the quartz block is rolling about the line of sight to the guide star with a period of 77.5 s, both of these signals are modulated at the satellite roll frequency. The star trackers on the spacecraft's attitude reference platform measure the phase of the roll to an accuracy better than 10 arcsec (50 μrad), so both the gyroscope readout and the telescope readout are demodulated using the measured roll phase.

During those periods of the orbit where the guide star is not occulted by the Earth (these periods are referred to as *guide star valid* periods), the attitude control system used the output of the science telescope to continuously point the telescope optical axis at the apparent direction to the guide star. This method of controlling the spacecraft kept the telescope readout within its ± 0.4 arcsec (2 μrad) linear range. Once the guide star was acquired, the spacecrafts attitude control system was typically able to maintain the guide star at the null position of the telescope readouts to within ± 0.2 arcsec (1 μrad). In addition, because of the careful initial alignment of the gyroscope spin axes relative to the guide star and the low gyroscope drift rate, the spin axes of each of the four gyroscopes remained within 30 arcsec (150 μrad) of the satellite roll axis over the course of the year. This close alignment reduced the sensitivity of the system to gyroscope scale factor uncertainty.

4˙1.1. Combined gyroscope and telescope signals for a single orbit. The gyroscope and telescope signals may be combined to determine the orientation of the gyroscope spin axis relative to the apparent direction to the guide star, as long as the ratio of the scale factors and the orientation of the telescope axis relative to the pickup loop are known. From measurements made during the assembly of the quartz block, the clocking of the plane of the pickup loop with each of the gyroscope readouts was known to an accuracy of better than 0.01 rad [53]. The normals to the pickup loops for gyroscopes 1 and 2 were aligned within one degree of the telescope X-axis, while the normals to the pickup loops for gyroscopes 3 and 4 were aligned within one degree of the telescope Y-axis. In this configuration, one telescope axis was the dominant contributor to the pointing errors in measurement of each gyroscope orientation.

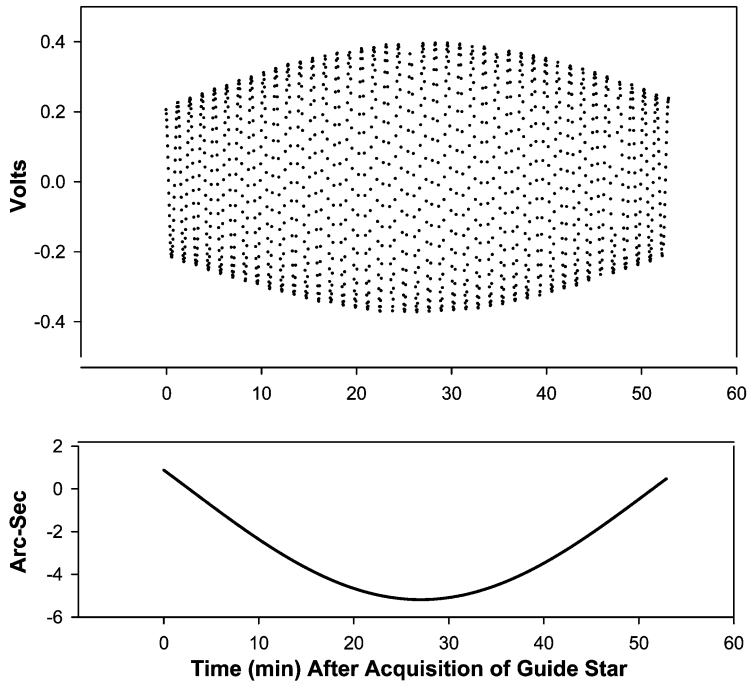

Fig. 11. – Combined gyroscope and telescope signals for a guide star valid period.

To determine the relative scale factor of the gyroscope and telescope readout systems, a sinusoidal dither signal was injected into the pitch and yaw axes of spacecraft's attitude control system. The spacecraft X-axis was commanded to dither at an amplitude of 60 mas with a period of 29 seconds, while the spacecraft Y-axis was commanded to dither at an amplitude of 60 mas with a period of 34 seconds. By measuring the amplitudes of the gyroscope and telescope readout signals at each of these two dither frequencies, the scale factor and orientation of the telescope readouts could be determined relative to each of the gyroscope readouts. With this knowledge, the telescope readout signals could be combined with each gyroscope readout signal to give a signal proportional to the misalignment between the gyroscope spin axis and the apparent direction to the guide star.

Figure 11 shows the combined gyroscope and telescope signal for one guide star valid period. The dominant signal lies at the satellite roll period of 77.5 s with its amplitude and phase modulated at the orbital period. The source of this modulation is the change in the apparent direction of the guide star because of the aberration of starlight, which provides a known calibration signal for the readout system. The aberration of starlight is due to changes in the velocity of the telescope relative to the direction to the guide star. An approximate expression may be found classically, but special relativity provides an exact treatment [54]. The component of aberration of starlight, which is modulated at the orbital frequency, is referred to here as the *orbital aberration*. It has a magnitude of approximately 5 arcsec (25 μrad) and varies sinusoidally in the plane of the orbit at the orbital period. Since the position and velocity of the spacecraft are known to a fractional accuracy of better than 10^{-5}, the orbital aberration signal is also known to this accuracy. The lower panel of this figure shows the magnitude of the aberration of

starlight due to the orbital motion of the spacecraft about the Earth is shown in the lower panel of fig. 11. For each orbit, this known orbital aberration signal may be used to find the scale factor of the gyroscope readout, C_g, and orientation of the pickup loop relative to the star trackers, $\delta\phi$. The result is a continuous and accurate calibration of the gyroscope and telescope readout systems.

For every orbit, the dominant contributions to the combined gyroscope and telescope signal are the orbital aberration and a roll frequency signal. The magnitude and phase of this roll frequency signal determines the orientation of the gyroscope spin axis relative to the apparent direction to the guide star. Known long-term changes in the apparent direction of the guide star are discussed below. After these effects are removed, the history of the gyroscope spin axis orientation relative to the true position of the guide star may then be found from the changes in the amplitude and phase of this roll frequency signal.

4˙1.2. Modulation of gyroscope readout scale factor due to trapped magnetic flux. For each of the gyroscopes, there is a small contribution of the trapped magnetic flux to the scale factor, C_g. Since the trapped flux is fixed in the body-fixed frame of the gyroscope, its contribution is modulated at the harmonics of the gyroscope polhode frequency. The largest magnitude of this modulation was 3% for gyroscope 1, the gyroscope closest to the telescope, and decreased to less than 0.4% for gyroscope 4, roughly corresponding to the residual trapped magnetic field discussed in chapter *magnetic flux reduction*, in subsubsect. **3**˙2.1. Over short intervals of up to several days, the amplitude of this modulation may be treated as constant, and the magnitude and phase of the modulation may be determined by fitting the data to a nonlinear model which includes the modulation coefficients as parameters.

Because of the changing polhode path in the gyroscope, the magnitude and phase of the modulation at each of the harmonics of the polhode frequency slowly change. In addition, there is a small but slowly varying contribution to the zero-frequency component of the gyroscope scale factor due to the trapped magnetic flux. As a result, the gyroscope readout scale factor may be determined to an accuracy of 3×10^{-4} over intervals of 5 days. Over longer intervals, it will likely be necessary to take advantage of the information provided by the high-frequency channel of the SQUID readout system as discussed in subsubsect. **2**˙1.1. The signals at harmonics of the gyroscope spin speed contain detailed information of the distribution of the trapped magnetic flux within each of the gyroscopes. Initial efforts at this mapping of the trapped magnetic flux have given promising results that may be used to further improve the accuracy of the gyroscope readout scale factor.

4˙1.3. History of the orientation of the gyroscope spin axis relative to the apparent position of the guide star. It is useful to define the coordinate systems used for the data analysis. The unit vector, $\boldsymbol{e}_{\rm S}$, is defined as the true direction to the guide star, while the $\boldsymbol{e}_{\rm R}$ is defined as the direction of the Earth's rotation axis on January 1, 2000. The unit vector in the West-East direction $\boldsymbol{e}_{\rm WE}$ is defined as the cross product of these two vectors

$$\boldsymbol{e}_{\rm WE} = \boldsymbol{e}_{\rm S} \times \boldsymbol{e}_{\rm R}. \tag{4˙1.3.1}$$

A third orthonormal basis vector in the North-South direction may be defined by the cross product

$$\boldsymbol{e}_{\rm NS} = \boldsymbol{e}_{\rm WE} \times \boldsymbol{e}_{\rm S}. \tag{4˙1.3.2}$$

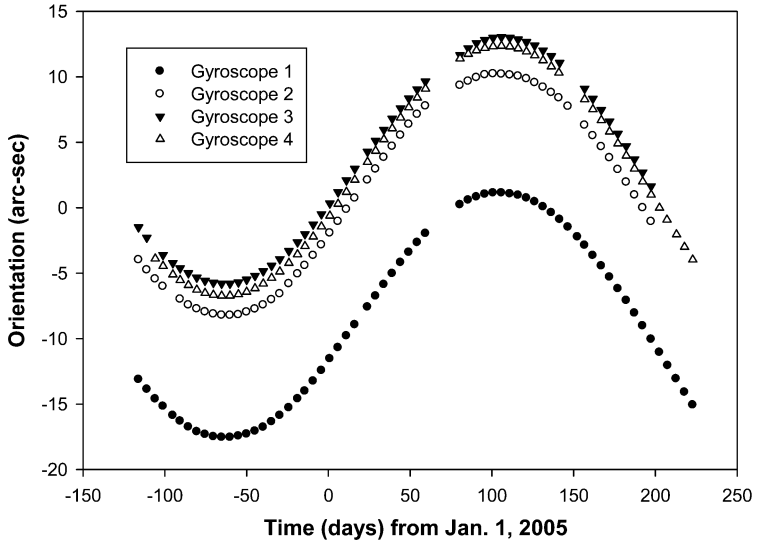

Fig. 12. – History of gyroscope spin axis orientation in the North-South direction.

The physical direction of each of the four gyroscope spin axes is nearly parallel or antiparallel to the direction to the guide star, but, for simplicity, the spin-axis direction may always be defined as lying nearly in the direction of the guide star. The component of this spin axis along the unit vector $\boldsymbol{e}_{\mathrm{NS}}$ is denoted by NS, while the component of the spin axis along the unit vector $\boldsymbol{e}_{\mathrm{WE}}$ is denoted by WE.

The measurement equation for the roll frequency components of the combined gyroscope and telescope signals, z_i at time t_i is

$$z_i = C_g \left\{ (NS_i - A_{\mathrm{NS}}) \cos(\phi_r + \delta\phi) + (WE_i - A_{\mathrm{WE}}) \sin(\phi_r + \delta\phi) \right\}. \tag{4·1.3.3}$$

Here, C_g is the scale factor of the combined gyroscope and telescope signals, ϕ_r is the roll phase as measured by the star trackers on the attitude reference platform, $\delta\phi$ is a fixed phase difference between the normal to the pickup loop and the star trackers, NS_i and WE_i denote the orientation of the components of the gyroscope spin axis at time t_i, and A_{NS} and A_{WE} are used to denote the combined effects of the aberration of starlight, deflection of starlight, parallax, and a displacement of the optical centroid of the guide star from the mass center of the binary system.

Figures 12 and 13 show the history of the orientation of each of the gyroscope spin axes relative to the apparent direction to the guide star. Each data point is the average orientation over a 5 day interval. For each of these data points, the scale factor and roll phase offset have been determined using the orbital aberration. For each 5 day interval, the time-averaged roll-frequency components of the combined gyroscope and telescope signals were also determined as well as the rate of change of these components. The scale factor and roll phase offset for each interval were then applied to the data to determine the physical orientation of each gyroscope.

The apparent direction to the guide star differs from the true direction to the guide star because of optical aberration due to the changing velocity of the spacecraft, the gravitational deflection of the light from the guide star by the Sun, and the parallax

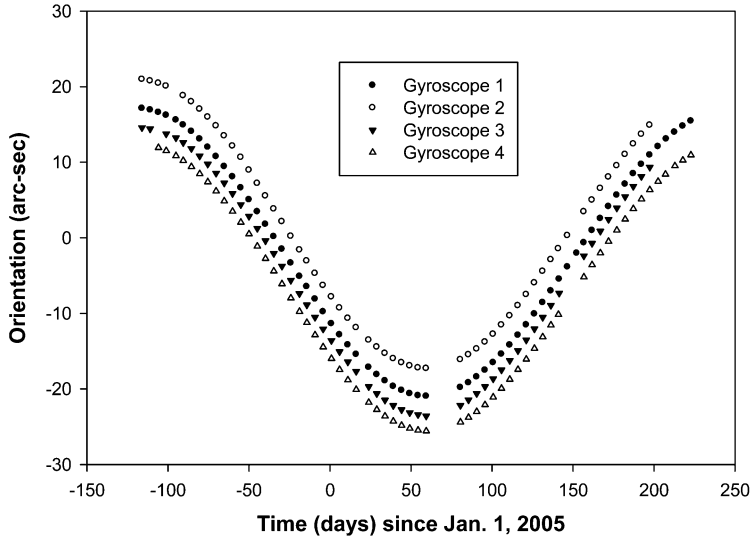

Fig. 13. – History of gyroscope spin axis orientation in West-East direction.

due to the Earth's annual motion about the Sun. In addition to the orbital aberration, there is another component of the aberration of starlight due to the annual motion of the Earth about the Sun, referred to as the *annual aberration*. This signal has a magnitude of 20 arcsec (100 μrad), and its direction slowly varies in an elliptical path as the component of the velocity of the Earth perpendicular to the line of sight to the guide star changes at the annual period. The magnitude and direction of this annual aberration were determined from the position and velocity of the Earth relative to the barycenter of the solar system as given by the JPL Earth ephemeris. Since the guide star lies at an ecliptic latitude of 22.1 degrees, the gravitational deflection of the light from the guide star by the Sun has a maximum magnitude of 21 marcsec (0.1 μrad), which occurs on March 11. The peak-to-peak magnitude of the parallax is approximately 10 mas (50 nrad). In the analysis described here, the annual aberration, deflection of light, and parallax were treated as known, but they can also, in principle, be determined independently from the data.

4˙1.4. History of gyroscope spin axis orientation relative to the true position of guide star. In figs. 12 and 13, it can be seen that the change in the orientation of each of the gyroscopes over the course of the year is dominated by the 20 arcsec (100 μrad) amplitude of the aberration of starlight due to orbital motion of the Earth about the Sun. The known effects of the annual aberration, deflection of starlight, and parallax may be subtracted from these measurements to give the orientation of the gyroscope spin axis relative to the true position of the guide star. The result is shown in figs. 14 and 15. The motion of the spin axes of all four gyroscopes has a drift rate of approximately 6.6 arcsec/y in the North-South direction, which is in good agreement with predicted geodetic drift rate. However, in the East-West direction, the drift rate is not constant which makes it difficult to compare it with the predicted frame-dragging effect.

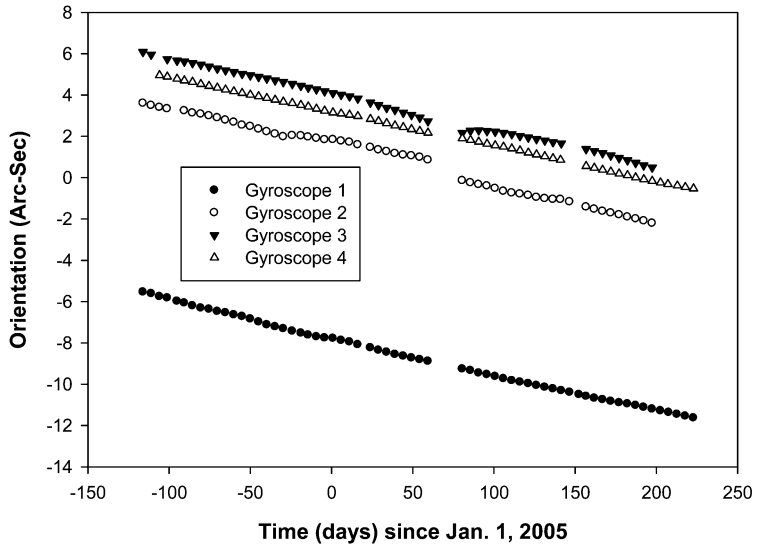

Fig. 14. – History of spin axis relative to true position of the guide star in the North-South direction.

4˙2. *Results from the calibration phase.* – These preliminary results indicate that there are additional effects which are not yet accounted for in the data analysis. One clear indication of additional classical torques acting on the gyroscopes was found during the calibration phase. The attitude control system of the spacecraft was commanded to

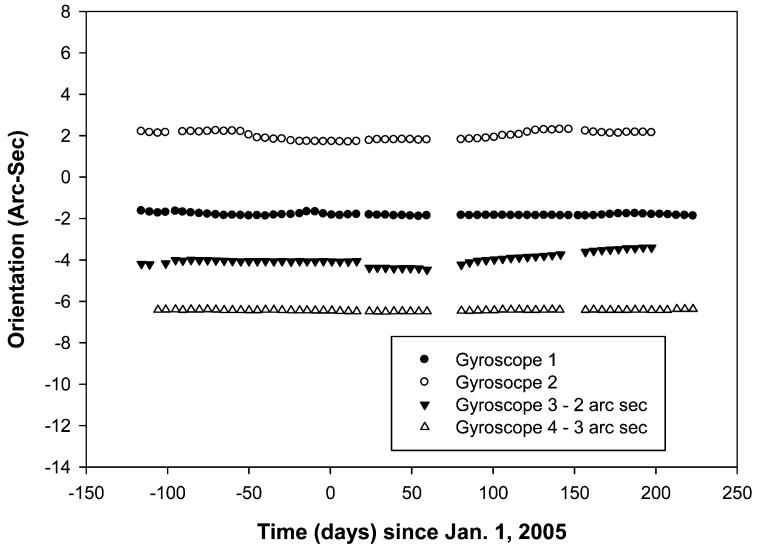

Fig. 15. – History of gyroscope spin axis orientation relative to the true guide star position in the West-East direction.

maneuver to a nearby star and to lock onto the alternate star for each portion of the orbit where the star was not occulted by the Earth. The spacecraft was maintained in this configuration for 24 h and then commanded to return to the guide star, IM Pegasi. The purpose of this operation was to increase the misalignment between the satellite roll axis and the spin axis of each of the gyroscopes. A comparison of the change in the orientation of the gyroscope before and after the maneuver may be used to place limits on any classical torques that are proportional to the misalignment between these two vectors. Because the initial results of these operations indicated that there were torques acting on the gyroscopes, which are significantly larger than expected, these spacecraft maneuvers were repeated 17 times under a variety of operating conditions. The spacecraft was maneuvered to lock onto stars as far as 7 degrees from IM Pegasi with the majority of maneuvers to stars or virtual stars within 1 degree of the guide star. In addition, the operating conditions of the spacecraft and the electrostatic suspension system were deliberately varied to find out how these operating conditions affected the measurements.

The analysis of the data from these maneuvers showed that for each of the gyroscopes there was a torque acting on the gyroscope which was proportional to the misalignment between the gyroscope spin axis and the spacecraft roll axis. In addition, the direction of the torque caused the gyroscope spin axis to precess about the direction of the satellite roll axis, or, in other words, the gyroscope drift rate was in an azimuthal direction about the satellite roll axis. The relation between the drift rate and the misalignment angle was linear to within 10% for misalignments less than 1 degree but became very nonlinear for larger misalignment angles. Deliberately commanded accelerations of the spacecraft up to $10^{-6}\,\mathrm{m/s^2}$ had very little effect on the magnitude or direction of the drift rate. In addition, increasing the preload voltage of the electrostatic suspension system from 0.2 V to 10 V had no measurable effect on the drift rate, but changing the operating mode of the electrostatic suspension system from a preload modulated at 20 Hz to a d.c. preload significantly changed the magnitude, but not the direction of these misalignment torques.

A clearer understanding of these misalignment torques came from a model of the effects of the electrostatic potentials on the surface of the rotor and the housing. It was clear from the magnitude of the torque that it could not be explained by the asphericity and mass unbalance of the conducting surfaces of the rotor and the housing interacting with the electric fields produced by the electrostatic suspension system and charges on the rotor and the housing. Instead, a more general model was constructed, which included patch effects on the surface of the rotor and the housing. The patch effect is usually described in terms of a surface dipole layer [55] above the underlying conducting surface, which produces electrostatic potential frozen on the surface, independent of external applied fields. In this case, the electric field is no longer necessarily perpendicular to the surface, and it is possible, under some circumstances to produce torques on a perfectly spherical rotor. Similar effects have been discussed for planar surfaces by Speake [56].

To investigate the potential torques acting on the gyroscope in this case, detailed calculations of the potential torques were made for an arbitrary distribution of the electrostatic potential on the surface of the rotor and the housing [57]. The electrostatic potentials on both the surface of the rotor and the housing were expanded in terms of spherical harmonics and transformed to a common reference frame using rotation matrices. Laplace's equation for the potential in the gap between the rotor and the housing was solved, and this solution was used to find the total energy in the electric field as a function of the orientation of the gyroscope spin axis. The torque may then be found by differentiating the energy stored in the electric field with respect to the Euler angles, which describe the orientation of the gyroscope spin axis. The resulting torque may be

averaged over the spin of the gyroscope and the roll of the satellite.

The resulting calculated torque agrees very well with the observations. If the angle, β, between the satellite roll axis and the gyroscope spin axis is small compared to the variations in the spherical harmonic expansion of the patch effect potential, then the magnitude of the torque averaged over the roll of the housing and the spin and polhode motion of the gyroscope is

$$\tau = \varepsilon_0 \frac{a^2}{2\Delta} \beta \sum_{l=\text{odd}}^{\infty} l(l+1) R_{l0} P_l(\cos\gamma) H_{l0}, \qquad \beta \ll 1, \tag{4·2.1}$$

where ε_0 is the permittivity of free space, a is the rotor radius, Δ is the gap between the housing and the rotor, and γ is the angle between the principal axis of the gyroscope corresponding to the maximum moment of inertia and the spin axis of the gyroscope. The coefficients in the spherical harmonic expansion of the electrostatic potential on the surface of the rotor in the principal axis reference frame are R_{lm} and coefficients in the expansion of the housing potential are H_{lm}, in a reference frame with the satellite roll axis along the z-axis. $P_l(\cos\gamma)$ denotes the Legendre polynomial of order l.

For small angular misalignments between the satellite roll axis and the gyroscope spin axis, the magnitude of the disturbance drift rate is proportional to the misalignment and its direction is perpendicular to the misalignment. It is proportional to the product of the coefficients of the spherical harmonic expansion of the rotor and housing potentials having the same order and increases with increasing order of the spherical harmonic. It is important to note that the torque is due to an interaction of the potential on the surface of the rotor with the potential on the surface of the housing. A patch effect potential on either surface alone produces no torque. Also, the interaction of the a.c. potential applied to the electrodes will produce no net torque since the 20 Hz modulation frequency is well averaged. As observed during the calibration phase, a d.c. potential applied to the electrodes will produce a torque on the gyroscopes, but this d.c. operating mode for the electrostatic suspension system was not used during the science data collection phase. Even though this model clearly explains the observed effects, some of the details of the interaction between the potentials on the housing and the rotor are not known. Although the effect could be explained by patch effect potentials on the surface of the rotor interacting with patch effect potentials on the surface of the housing, additional contributions may results from the patch effect potentials on the surface of the rotor interacting with holes in the gyroscope housing.

This model of the interaction of the patch effect fields on the surface of the rotor and the surface of the housing also explains an additional observation. At those times when a harmonic of the rotor's polhode frequency coincided with satellite roll frequency, offsets in the gyroscope spin axis as large as 0.1 arcsec occurred over intervals of approximately one day. As the harmonic of the slowly changing polhode frequency drifts through the roll frequency, there is a torque which has a nonzero average value [57]. In this case, the orientation of the gyroscope spin axis follows a Cornu spiral, which can be separated from the uniform drift rate because of its unique time signature.

4·3. *Data analysis in the presence of misalignment torques.* – One important question is whether the gyroscope drift rate due to these misalignment torques can be clearly separated from the relativistic drift rate. At any given time, the gyroscope drift rate may be divided into two components: one component in a direction parallel to the misalignment between the gyroscope spin axis and the satellite roll axis (the radial component) and the

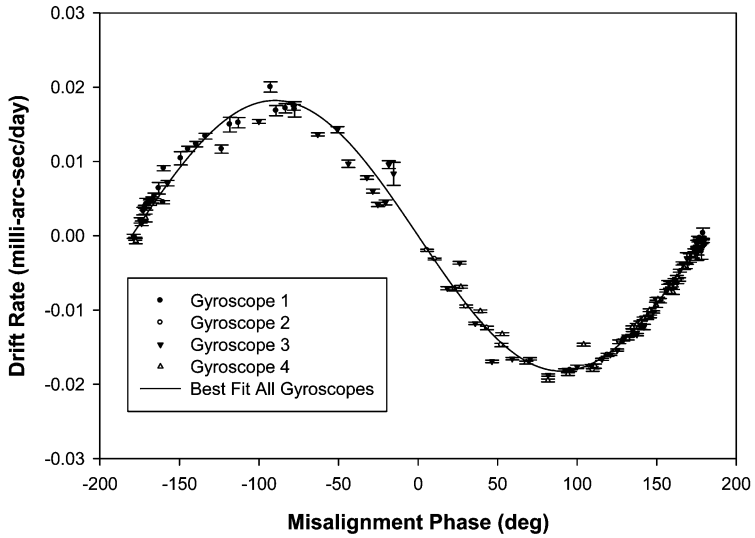

Fig. 16. – Radial drift rate *vs.* misalignment phase for all four gyroscopes.

other component in a direction perpendicular to the misalignment between the gyroscope spin axis and the satellite roll axis (the azimuthal component). The azimuthal component of the drift rate has contributions from the misalignment torque and the relativistic drift rate, but the radial component is entirely due to the relativistic drift rate. As the direction of the misalignment changes, primarily due to the annual aberration, a uniform relativistic drift rate will vary sinusoidally as a function of the misalignment phase (the direction of the misalignment in an inertial reference frame). The amplitude of the sine wave is equal to the magnitude of the relativistic drift, while the phase of the sinusoidal variation determines the direction of the uniform, relativistic drift rate. A plot of the radial component of the drift rate *vs.* the misalignment phase is shown in fig. 16. Data was not used at those times when a harmonic of the polhode frequency was close to the roll frequency.

Although this method of analyzing the flight data shows that the relativistic drift rate may be clearly separated from the effects of the misalignment torque, other methods of analyzing the data will very likely be more accurate. To apply this method, the data is divided into segments several days long and the drift rate for each segment is determined. Dividing the data into short segments decreases the potential accuracy advantage of the drift rate estimates decreasing as $1/T^{3/2}$ where T is the measurement time. On the other hand, if the misalignment torques and the relativistic drift rate are simultaneously estimated, there is no limitation due to the short data segments. Initial efforts to simultaneously estimate these two effects have shown promising results.

5. – Conclusion

As of July, 2007, the data analysis gives a drift rate of -6638 ± 97 marcsec/y in the plane of the orbit (North-South direction). This result may be compared with the predicted uniform drift rate in the North-South direction of 6571 ± 1 marcsec/y. This drift rate includes the predicted terrestrial geodetic effect for the measured orbit of the Gravity

Probe B satellite, a contribution from the predicted solar geodetic, and the proper motion of the guide star. The measurement error is dominated by systematic errors as indicated by the disagreement between the measured drift rates of the four gyroscopes. At this time, the estimate for the drift rate in the West-East direction is consistent with frame-dragging effect predicted by general relativity, but additional work is needed before clear comparison between the measurements and the predicted effect may be made. There is significant room for improvement in the accuracy, and the estimated error will decrease as the data analysis progresses. Updates on the status of the data analysis at the end of 2008 may be found in refs. [57-61].

* * *

We would like to acknowledge the enormous contribution to this work by numerous people at Lockheed-Martin Space Corporation, NASA's Marshall Space Flight center, and Stanford University. This work was supported by NASA under contract number NAS8-39225. The authors would also like to acknowledge the generous support of R. D. Fairbank.

REFERENCES

[1] Pugh G. E., WSEG Research Memorandum Number 11 (Weapons Systems Evaluation Group, The Pentagon, Washington, D. C., November 12, 1959).
[2] Schiff L. I., *Proc. Nat. Acad. Sci.*, **46** (1960) 871.
[3] Schiff L. I., *Phys. Rev. Lett.*, **4** (1960) 215.
[4] Adler R. J. and Silbergleit A. S., *Int. J. Theor. Phys.*, **39** (2000) 1291.
[5] De Sitter W., *Mon. Not. R. Astron. Soc.*, **77** (1916) 155.
[6] Lense J. and Thirring H., *Z. Phys.*, **19** (1918) 156.
[7] Mashhoon B., Hehl F. W. and Theiss D. S., *Gen. Relat. Gravit.*, **16** (1984) 711.
[8] Thorne K. S., in *Near Zero: New Frontiers of Physics*, edited by Fairbank J. D. *et al.* (W. H. Freeman and Co., New York) 1988, pp. 573-586.
[9] Kasevich M. *et al.*, *Proceedings of the International School of Physics "Enrico Fermi", Course CLXVIII "Atom Optics and Space Physics"* edited by E. Arimondo, W. Ertmer, W. P. Schleich and E. M. Rasel (IOS Press, Amsterdam and SIF, Bologna) 2009, p. 411.
[10] Everitt C. W. F., in *Conference on Experimental Tests of Gravitational Theories*, edited by Davies R. W. (JPL) 1970, pp. 68-81.
[11] Debra D. B., in *Conference on Experimental Tests of Gravitation Theories*, edited by Davies R. W. (JPL) 1970, 190.
[12] Lange B., *AIAA Journal*, **2** (1964) 1590.
[13] Everitt C. W. F., in *Near Zero: New Frontiers in Physics*, edited by Fairbank J. D. *et al.* (W. H. Freeman and Co., New York) 1988, pp. 587-639.
[14] Lebach D. E. *et al.*, *Astrophys. J.*, **517** (1999) L43.
[15] See, for example, Ransom R. R. *et al.*, in *Future Directions in High Resolution Astronomy: The 10th Anniversary of the VLBA*, edited by Romney J. D. and Reid M. J. (ASP Conference Series), pp. 506-510.
[16] Lestrade J.-F. *et al.*, *Astron. Astrophys.*, **344** (1999) 1014.
[17] Everitt C. W. F., *Bull. Am. Phys. Soc.*, **52** (2007) A1.0001.
[18] Everitt C. W. F. *et al.*, in *First William Fairbank Conference on Relativistic Gravitational Experiments in Space*, edited by Demianski M. and Everitt C. W. F. (World Scientific, Singapore) 1993, pp. 309-323.
[19] Turneaure J. P. *et al.*, *Adv. Space Res.*, **9** (1989) 29.
[20] Turneaure J. P. *et al.*, *Adv. Space Res.*, **32** (2003) 1387.
[21] De Freitas J. M. and Player M. A., *Appl. Phys. Lett.*, **66** (1995) 3552.
[22] Lipa J. and Siddall G. J., *Precis. Eng.*, **2** (1980) 123.

[23] Gill D., Peters P. and Sisk C., *Surf. Coating Tech.*, **36** (1988) 471.
[24] Zhou P. *et al.*, *Surf. Coating Tech.*, **54/55** (1992) 548.
[25] Zhou P. *et al.*, *Surf. Coating Tech.*, **77** (1995) 516.
[26] Bracken T. D. and Everitt C. W. F., *Adv. Cryog. Eng.*, **13** (1968) 168.
[27] Becker R., Sauter F. and Heller G., *Z. Phys.*, **85** (1933) 772.
[28] London F., *Superfluids, Macroscopic Theory of Superconductivity*, Vol. **I** (Dover Publications, New York) 1960.
[29] Muhlfelder B., Lockhart J. M. and Gutt G. M., *Adv. Space Res.*, **32** (2003) 1397.
[30] Simmonds M., private communication (1995).
[31] Bencze W. J. *et al.*, in *Proceedings of the SIBC Annual Conference* 2003, pp. 1593-1598.
[32] Buchman S. *et al.*, *Rev. Sci. Instrum.*, **66** (1995) 120.
[33] Gwo D.-H. *et al.*, *Adv. Space Res.*, **32** (2003) 1402.
[34] Wang S. *et al.*, *Proceedings of the SPIE, Cryogenic Optical Systems and Instruments X*, **5172** (2003) 108.
[35] Wang S. *et al.*, in *Proceedings of the 24th International Conference on Low Temperature Physics* 2006, p. 1621.
[36] Gwo D.-H., *Ultra precision and reliable bonding method*, U. S. Patent 6284085, (2001).
[37] Sullivan M. T. *et al.*, *Proceedings of the SPIE - The International Society for Optical Engineering*, **3132** (1997) 56.
[38] Chilese F. C., *Adv. Cryog. Eng.*, **41** (1996) 1203.
[39] Buchman S. *et al.*, *Class. Quantum. Grav.*, **13** (1996) A185.
[40] Turneaure J. P. *et al.*, in *Near Zero: New Frontiers of Physics*, edited by Fairbank J. D. *et al.* (W. H. Freeman and Co., New York) 1988, pp. 671-678.
[41] Parmley R. T. *et al.*, *Proceedings of SPIE*, **619** (1986) 126.
[42] Parmley R. T. *et al.*, *Adv. Space Res.*, **32** (2003) 1407.
[43] Selzer P. M., Fairbank W. M. and Everitt C. W. F., *Adv. Cryog. Eng.*, **16** (1970) 277.
[44] Cabrera B. and Van Kann F. J., *Acta Astron.*, **5** (1978) 125.
[45] Cabrera B., in *Near Zero: New Frontiers in Physics*, edited by Fairbank J. D. *et al.* (W. H. Freeman and Co., New York) 1988, 312.
[46] Mester J. C. and Lockhart J. M., *Czech. J. Phys.*, **46** (1970) Suppl. S, 2751.
[47] Mester J. C. *et al.*, *Adv. Space Res.*, **25** (2000) 1205.
[48] Shestople P. *et al.*, in *Proceedings of the GNSS Meeting* (Institute of Navigation) 2004.
[49] Murray D. O., Taber M. A. and Burns K. M., in *2005 Cryogenic Engineering Conference and International Cryogenic Materials Conference* August 29-September 2, 2005.
[50] Hanuschak G. *et al.*, in *GNSS 2005* (Institute of Navigation).
[51] Li J. *et al.*, *Adv. Space Res.*, **40** (2007) 1.
[52] Bencze W. J. *et al.*, in *29th Guidance and Control Conference* (American Astronautical Society) 2006.
[53] Turneaure J. P., *Verification of Science Instrument Assembly Alignment Requirements*, S0376 Rev. A (Gravity Probe B, Stanford University) June 17, 2001.
[54] Stumpff P., *Astron. Astrophys.*, **78** (1979) 229.
[55] Darling T. W., *Electric Fields on Metal Surfaces at Low Temperatures* (University of Melbourne) 1989.
[56] Speake C. C., *Class. Quantum. Grav.*, **13** (1996) A291.
[57] Keiser G. M., Kolodziejczak J. and Silbergleit A. S., to be published in *Space Sci. Rev.* (2010).
[58] Everitt C. W. F. *et al.*, to be published in *Space Sci. Rev.* (2010).
[59] Muhlfelder B. *et al.*, to be published in *Space Sci. Rev.* (2010).
[60] Heifetz M. *et al.*, to be published in *Space Sci. Rev.* (2010).
[61] Silbergleit A. *et al.*, to be published in *Space Sci. Rev.* (2010).